https://doi.org/10.5194/bg-2022-230
Preprint. Discussion started: 9 December 2022

Biogeosciences Discussions

^{17}O-excess of grass phytoliths record daytime air relative humidity at a natural Mediterranean site

Claudia Voigt[1,2], Anne Alexandre[1], Ilja M. Reiter[3], Jean-Philippe Orts[4], Christine Vallet-Coulomb[1], Clément Piel[5], Jean-Charles Mazur[1], Julie Aleman[1], Corinne Sonzogni[1], Helene Miche[1], Jérôme Ogée[6]

[1]Aix Marseille Université, CNRS, IRD, INRAE, CEREGE, 13545 Aix-en-Provence, France
[2]Present address: University of Almería, Department of Biology and Geology, 04120 Cañada de San Urbano, Almería, Spain
[3]Research Federation ECCOREV, FR3098, CNRS, 13545 Aix-en-Provence, France
[4]IMBE, CNRS, Université d'Avignon, Aix-Marseille Université, IRD, 13397 Marseille, France
[5]ECOTRON Européen de Montpellier, UAR 3248, CNRS, Campus de Baillarguet, 34980 Montferrier-sur-Lez, France
[6]INRAE, Bordeaux Sciences Agro, UMR ISPA, 33140 Villenave d'Ornon, France

Correspondence to: Claudia Voigt (cvoigt@ual.es), Anne Alexandre (alexandre@cerege.fr)

Abstract

The triple oxygen isotope composition of phytoliths (^{17}O-excess$_{phyto}$) can provide key information on past atmospheric relative humidity (RH) over land. Here, we examined how leaf-to-air temperature gradients and changes in the silica polymerization rate in response to stomatal conductance influence the interpretation of ^{17}O-excess$_{phyto}$ in terms of RH. Further, we assessed the reliability of a theoretical isotope model of leaf water evaporation to predict the triple oxygen isotope composition of leaf water on diurnal and seasonal scale. For this purpose, we monitored a grass plot within a natural Mediterranean woodland for one year. We measured in particular the isotope composition of atmospheric water vapor and plot-scale grass leaf temperatures – two variables that are often only estimated. Grass leaf blades were collected in different seasons and over a 24-hour period for leaf water and phytolith isotope analysis. We found that the steady state model reliably predicts the triple oxygen isotope composition of leaf water during daytime but remains sensitive to uncertainties on the leaf-to-air temperature difference. Deviations from isotope steady state at night are well represented by the non-steady state model. In our study, the ^{17}O-excess$_{phyto}$ best reflects average daytime RH over the growth period, rather than daily RH. Average daytime leaf-to-air temperature gradients of less than 2 °C introduce an insignificant bias to the RH estimate. The results also confirm the established triple oxygen isotope fractionation factors between phytoliths and leaf water. The findings of this study help to better understand how to interpret ^{17}O-excess$_{phyto}$ of fossil phytolith assemblages in terms of past RH.

1 Introduction

Continental atmospheric relative humidity (RH) is a key factor of soil evaporation, transpiration, dryness stress and ecosystem productivity (Liu et al., 2021; López et al., 2021; Grossiord et al., 2020). However, RH is estimated with low precision in the Earth system models (IPCC, 2013; Tierney et al., 2020). Long-term data beyond the instrumental period is needed to improve

https://doi.org/10.5194/bg-2022-230
Preprint. Discussion started: 9 December 2022


Biogeosciences Discussions Open Access EGU

the representation of RH in these models. A few quantitative indicators of past RH available for model-data comparisons exist. During plant transpiration, leaf water undergoing evaporation imprints its isotope composition on leaf organic and mineral compounds formed during plant growth, such as cellulose, n-alkanes of leaf waxes, or phytoliths. After plant death, these compounds can be preserved in soils and sediments and used as past climate indicators. Relationships between their isotope composition (δ^2H, $\delta^{18}O$, and recently $\delta^{17}O$) and current climate parameters, including RH, were calibrated for the purpose of past climate reconstructions (Helliker and Ehleringer, 2002a, b; Kahmen et al., 2011, 2013; Zech et al., 2014; Tuthorn et al., 2015; Alexandre et al., 2018, 2019; Outrequin et al., 2021; Garcin et al., 2012). However, these observations have often been performed in controlled environmental conditions, not representative of the diurnal, daily and seasonal climate variations encountered in the natural environment. Therefore, the question of the time span (seasonal vs annual, diurnal vs daily) integrated by these isotope indicators still remains open.

Leaf waters generally show higher δ^2H, $\delta^{18}O$, and $\delta^{17}O$ and lower d-excess [$= \delta^2H - 8\,\delta^{18}O$] and ^{17}O-excess [$= \delta'^{17}O - 0.528\,\delta'^{18}O$ with $\delta' = 1000\ln(\delta/1000+1)$] than meteoric waters due to significant evaporative fractionation during transpiration. The magnitude of this isotope fractionation can be predicted by the isotope-evaporation model developed by Craig and Gordon (1965), and later adapted to leaf transpiration (Dongmann et al., 1974; Farquhar and Cernusak, 2005). This model (hereafter referred to as the C-G model) considers three main processes occurring in the boundary layer of the leaf during transpiration: liquid water-water vapor equilibrium at the boundary layer interface, diffusion of water vapor from the evaporative sites in the leaf to the surrounding air, and back-diffusion of atmospheric water vapor to the leaf (Craig and Gordon, 1965; Farquhar et al., 2007; Cernusak et al., 2016). The C-G model is based on the steady-state assumption, i.e. all water that is lost by evaporation is continuously replenished by xylem water. This assumption neglects small diurnal changes in leaf water content that are expected to result in only 3 % error in the predicted leaf water $\delta^{18}O$ enrichment (Farquhar and Cernusak, 2005; Farris and Strain, 1978). The C-G model also assumes isotope steady state, so that the isotope composition of transpired water matches that of source (xylem) water (R_S). In this situation, the isotope ratio of the evaporated water pool in the leaf (R_e) is (Craig and Gordon, 1965; Dongmann et al., 1974; Farquhar et al., 2007; Cernusak et al., 2016):

$$R_e = \alpha_{eq}\alpha_{diff}(1-h)R_S + \alpha_{eq}hR_V, \quad (1)$$

where R_V denotes the isotope ratio of atmospheric water vapor and h is the ratio of the actual vapor pressure in the atmosphere to the saturation vapor pressure inside the leaf (i.e. at leaf temperature, T_{leaf}). When the leaf-to-air temperature gradient is small, h is equal to RH.

Although the C-G model reproduces the observed trends in the isotope composition of bulk leaf water, discrepancies between modeled and observed values as high as 6 ‰ for $\delta^{18}O$ (e.g., Flanagan et al., 1991; Gan et al., 2002; Song et al., 2015; Loucos et al., 2014; Cernusak et al., 2016; Bögelein et al., 2017) and higher than 100 per meg for ^{17}O-excess (Li et al., 2017; Alexandre et al., 2018; Outrequin et al., 2021) have been reported. Some of these studies neglected that bulk leaf water ($R_{leaf,ss}$) is a mixture of two water pools: an evaporated water pool in the lamina mesophyll whose isotope composition is predicted by the C-G

https://doi.org/10.5194/bg-2022-230
Preprint. Discussion started: 9 December 2022

model (R_e, Eq. (1)), and an unevaporated pool in the leaf veins and associated ground tissues, whose isotope composition matches R_s (Leaney et al., 1985; Yakir et al., 1994; Hirl et al., 2019):

$$R_{leaf,ss} = (1 - f)R_e + fR_s \quad (2)$$

where f represents the water volume fraction of the unevaporated pool. Incomplete isotope mixing within the leaf lamina mesophyll, resulting from a limited back-diffusion of enriched water from the evaporative sites opposed to the advection of depleted xylem water to those sites, has also been proposed as possible explanations for the discrepancies between modelled R_e (Eq. (1)) and observed R_{leaf} (Farquhar and Lloyd, 1993; Farquhar et al., 2007; Holloway-Phillips et al., 2016). Such incomplete mixing would result in formulations similar to Eq. (2), but with a dependency of f on the transpiration rate that is difficult to gather (Hirl et al., 2019; Barbour et al., 2021).

From Eqs. (1) and (2), we can see that, if f is constant and not too close to unity (a typical value for grass species is around 0.2–0.4, see Hirl et al. (2019) and Barbour et al. (2021)), diurnal changes in $R_{leaf,ss}$ are dominated by changes in R_e. Changes in R_e are almost linearly related to changes in h, provided that the temporal variations of other factors (R_s, R_v, α_{diff}, α_{eq}) are limited. Thus, any isotope marker that imprints the isotope signal of bulk leaf water (R_{leaf}) is also a tracer of past changes in h or RH. Given the often-large diurnal and seasonal variations in RH, it is crucial to know the exact timing of this isotope signal imprint. For example, in the desiccant-tolerant moss *Syntrichia ruralis*, the carbon and oxygen isotope composition of cellulose suggested a temporal separation between photosynthesis and growth, whereby CO_2 assimilation occurred at low relative water content, while cellulose synthesis occurred during conditions of high relative water content (i.e. at night or during rain) (Royles et al., 2013). Further, deviations from isotope steady state resulting from low stomatal conductance (g_s) and transpiration rate and thus long leaf water residence time in the mesophyll cells are common, notably at night or during drought (Cuntz et al., 2007; Ogée et al., 2007; Cernusak et al., 2016; Wang et al., 2018). These non-steady state conditions may complicate the interpretation of the isotope markers and need to be accounted for.

Discrepancies between isotope measurements and C-G model predictions can also arise from uncertainties in key parameters of the C-G model that are difficult to measure, such as the isotope composition of atmospheric water vapor and the difference between leaf temperature and air temperature ($\Delta T_{leaf\text{-}air}$) (Cernusak et al., 2002; Flanagan and Farquhar, 2014; Li et al., 2017; Alexandre et al., 2018). $\Delta T_{leaf\text{-}air}$ determines h and influences the equilibrium fractionation factor α_{eq}, and consequently predictions of $\delta^{18}O$, δ^2H, and d-excess of bulk leaf water. The ^{17}O-excess of bulk leaf water is less affected by $\Delta T_{leaf\text{-}air}$ given the low temperature-dependency of the triple oxygen isotope equilibrium fractionation between liquid water and water vapor (θ_{eq} equals to 0.529 over the temperature range 11.4–41.5 °C; Barkan and Luz, 2005) and the proximity of θ_{eq} to 0.528, which is the slope of the Global Meteoric Water Line (GMWL) considered in the definition of the ^{17}O-excess (Luz and Barkan, 2010). Therefore, the ^{17}O-excess of bulk leaf water is essentially controlled by the diffusion of water vapor in air (θ_{diff} equals to 0.518; Barkan and Luz, 2007), and the isotope exchange between leaf water at the evaporative sites and atmospheric water vapor. The extent of both processes depends mainly on h. Consequently, the ^{17}O-excess of bulk leaf water should be more prone to

https://doi.org/10.5194/bg-2022-230
Preprint. Discussion started: 9 December 2022

detect the exact timing of h or RH than $\delta^{18}O$, $\delta^{2}H$, and d-excess that are additionally influenced by changes in temperature. In addition, compared to $\delta^{18}O$, $\delta^{2}H$, or d-excess, the ^{17}O-excess is less variable in meteoric water, which feeds the soil water taken up by the plants, and is also assumed to vary little in atmospheric water vapor (Luz and Barkan, 2010; Surma et al., 2021; Aron et al., 2021). Recent calibration studies in growth chambers and at natural sites demonstrated that the ^{17}O-excess of phytoliths ($^{17}O\text{-excess}_{phyto}$), inherited from the ^{17}O-excess of leaf water, is controlled by RH around the plant, according to a gradient of 4.3 ± 0.3 per meg $\%^{-1}$. This relationship has been found to be independent of grass leaf length and vegetation type (Alexandre et al., 2018, 2019; Outrequin et al., 2021). Further, the $^{17}O\text{-excess}_{phyto}$ has been shown to be weakly affected by changes in air temperature or atmospheric CO_2 levels (Outrequin et al., 2021). Whether these findings from controlled experiments are valid in the natural environment is still an open question.

In this study, a grass plot within the understory of a natural Mediterranean downy oak forest was equipped to measure for the course of one year, all environmental and plant physiological parameters relevant for modelling the triple oxygen isotope composition of the grass leaf water and phytoliths. In particular, the triple oxygen and hydrogen isotope composition of atmospheric water vapor above the grass was measured continuously over the year using a cavity ring-down spectrometer (CRDS), and plot-scale grass leaf temperature (T_{plot}) was monitored using an infra-red (IR) radiometer. Grass leaves were collected at midday on eight days in different seasons and over a 24-hour period in June for triple oxygen and hydrogen isotope analyses of bulk leaf water. Through a model-data approach, we re-examined the parameters determining the triple oxygen isotope compositions of bulk leaf water. In addition, grass leaves were harvested in spring, summer and autumn for phytolith extraction and triple oxygen isotope analysis to examine which RH average is recorded in $^{17}O\text{-excess}_{phyto}$ of phytolith assemblages that are formed over growth periods of several months. Further, we investigate the relationship between the triple oxygen isotope composition of phytoliths and leaf water to assess the potential of fossil phytoliths for reconstructing past changes in leaf water.

2 Materials & Methods

2.1 Experimental setup

The AnaEE in natura experimental platform O_3HP is located about 100 km north of Marseille (France) at an altitude of 680 m above sea level (43.935° N, 5.711° E). On 14 February 2021, the grass species *F. arundincaeae*, also referred to as tall fescue, was sown (8 g m^{-2}) on a 5.5 m^2 plot in the understory of an oak-dominated woodland. Potting soil was added to the shallow calcaric leptosol (IUSS Working Group WRB, 2015; Belviso et al., 2016) and supplied with ~ 50 g m^{-2} organic fertilizer (Engrais Gazon, Neudorff, Emmerthal, Germany) and 2.7 g m^{-2} SiO_2 (General Hydroponics Mineral Magic, Terra Aquatica, Fleurance, France) to ensure a sufficient amount of nutriments and bio-available silica.

The experimental plot was automatically irrigated with tap water (30 mm d^{-1}) from 04 March 2021 until the end of the experiment on 23 November 2021 to avoid water stress in the grasses. The potential evaporation from the grass plot estimated

https://doi.org/10.5194/bg-2022-230
Preprint. Discussion started: 9 December 2022


Biogeosciences Discussions Open Access EGU

using the Penman-Monteith equation (Monteith, 1965) was an order of magnitude lower than the irrigation rate, ranging from 2–4 mm d^{-1}. Therefore, we assume that soil water evaporation was negligible and had no impact on the isotope composition of leaf water. An aliquot of the irrigation water was collected in an evaporation-free water collector (Rain Sampler 1, Palmex d.o.o., Zagreb, Croatia; Gröning et al., 2012), that was sampled weekly. Precipitation was collected on an event-based interval using a second water collector of the same type. Both collectors were emptied and dried each time after sampling. For isotope analysis of atmospheric water vapor, the air at 0.4 m above the grass plot was pumped continuously (N 86 KN.18, KNF DAC GmbH, Hamburg, Germany) to a Picarro L2140-i CRDS (Picarro Inc., California, USA), installed in an air-conditioned cabin on the experimental site. The air was passed through a 11.5 m long and 1/4 " wide PFA tube (PFA-T4-062-100, Swagelok, Ohio, USA), at a flow rate of 5 L min^{-1}. The tubing was insulated and heated to prevent condensation of the water vapor. A funnel covered by a net was placed at the inlet for protection from rain and suction of insects and large aerosol particles.

The following climate parameters were measured on the experimental site: Global solar radiation at 6 m above ground (LI-200, LI-COR Biosciences Inc., Nebraska, USA), precipitation amount (15189 H, LAMBRECHT meteo GmbH, Göttingen, Germany), RH and T_{air} at 60 cm height next to the grass plot (HMP155, Vaisala Oyj, Vantaa, Finland), atmospheric temperature at 5 cm above the ground (T_{ground}) (DTS12, Vaisala Oyj, Vantaa, Finland), soil water content and soil temperature at ~ 5 cm depth (CS655, Campbell Scientific Inc, Logan, Utah, USA), plot-scale grass leaf temperature (T_{plot}) (IR radiometer SI-411-SS, Apogee Instruments Inc., Utah, USA), and sky temperature (T_{sky}). T_{plot} is the temperature integrated over the field of view of the IR radiometer that covered ~ 90 % of the grass plot surface. Each parameter was extracted in hourly resolution from the COOPERATE database (COOPERATE database, 2022).

On sampling days, stomatal conductance (g_s) and transpiration, were monitored continuously over the day on a single grass leaf of 4–5 mm width using a Li-6400 XT gas exchange system (LI-COR Biosciences Inc., Nebraska, USA). To assess the spatial variability of g_s, this parameter was additionally measured hourly on the adaxial side of ten leaves of at least 3 mm width, randomly selected on the plot, using an AP4 porometer (Delta-T Devices LTD, Cambridge, UK). In addition, leaf temperature (T_{leaf}) was measured in situ on the adaxial side of ten grass leaves, randomly selected, in one-hour intervals using an Optris CT IR thermometer (Optris GmbH, Berlin, Germany). T_{plot} and T_{leaf} measurements were corrected for emissivity of the grass canopy, considering the tree canopy gap fraction:

$$T_{plot}\ or\ T_{leaf} = \sqrt[4]{\frac{T_{raw}{}^4 - (1-\varepsilon)\cdot(\alpha \cdot T_{sky} + (1-\alpha)\cdot T_{canopy})^4}{\epsilon}} \quad (3)$$

where ε is the emissivity of the grass canopy (ε = 0.95; Apogee Instruments Inc, 2022) and α is the tree canopy gap fraction, which is estimated to be 0.3 throughout the experimental period. T_{raw} is the temperature recorded by the sensor, T_{sky} is the sky temperature and T_{canopy} is the canopy temperature, which is assumed to equal ambient air temperature.

https://doi.org/10.5194/bg-2022-230
Preprint. Discussion started: 9 December 2022

2.2 Sampling

F. arundinacea leaf samples were collected at midday on eight days in May, July, August, October, and November 2021 (Table 1), as well as every ~ 1.5 h over a 24-hour period from 14–15 June 2021. About ten leaf blades from different tillers evenly distributed over the grass plot were immediately transferred to 12 mL Exetainer vials (Labco, High Wycombe, UK), and stored in a fridge until water extraction and isotope analysis.

Three grass regrowths were monitored in spring (17 February–20 May 2021), summer (15 June–27 August 2021), and autumn (27 August–23 November 2021) (Table 2). Each regrowth started after the grasses had been cut above the sheath at 2–4 cm height. Grass heights were measured at monthly intervals. At the end of each regrowth, the grass leaves were harvested, dried at 50 ºC and kept for phytolith extraction and analysis.

https://doi.org/10.5194/bg-2022-230
Preprint. Discussion started: 9 December 2022

Biogeosciences Discussions Open Access EGU

Table 1: *F. arundinacea* leaf water isotope composition, *F. arundinacea* stomatal conductance (g_s) and transpiration (E), atmospheric temperature (T_{air}) and relative humidity (RH) at 60 cm height next to the grass plot, plot-scale grass leaf temperature (T_{plot}), atmospheric vapor pressure at 60 cm height (e_a), saturation vapor pressure at T_{plot} (e_i) and h = e_a/e_i, averaged over 30 minutes before sampling on 8 days at midday between May and November 2021 and 14 samplings during a 24-hour period from 14–15 June 2021. The sample ID indicates 'sampling location_plant_species_sample type_sampling date_sampling time'. Plant species 'FA' denotes Festuca arundinacea, sampling date is in the format YYYYMMDD and sampling time in UTC. SD = 1 standard deviation, $\Delta T_{leaf\text{-}air} = T_{plot}\text{-}T_{air}$.

Sample ID	E (mol m^{-2} s^{-1})	g_s (mol m^{-2} s^{-1})	T_{air} (°C)	T_{plot} (°C)	$\Delta T_{leaf\text{-}air}$ (°C)	RH (%)	h (%)	$\delta^{18}O$ (‰)	^{17}O-excess (per meg)	d-excess (‰)
Midday samples										
O3HP_FA_leaf_20210503_1130	2.5	0.097	17	18	0	42	42	9.87	-122	-88.5
O3HP_FA_leaf_20210520_1130	2.2	0.114	20	19	-2	36	40	20.09	-165	-142.8
O3HP_FA_leaf_20210722_1155	3.7	0.084	33	30	-3	27	32	12.53	-156	-99.3
O3HP_FA_leaf_20210826_1140	1.3	0.049	27	24	-3	42	50	4.47	-77	-52.3
O3HP_FA_leaf_20210827_1130	–	–	25	23	-2	38	43	6.37	-103	-59.3
O3HP_FA_leaf_20211022_1130	–	–	17	15	-2	65	74	3.19	-52	-36.3
O3HP_FA_leaf1_20211027_1130	1.1	0.107	16	15	-2	64	71	2.80	-43	-34.4
O3HP_FA_leaf_20211123_1230	1.4	0.127	14	12	-2	62	71	-0.05	17	-31.0
O3HP_FA_leaf2_20211123_1230	1.4	0.127	14	12	-2	62	71	1.63	-3	-42.6
24-hour period										
O3HP_FA_leaf_20210614_1720	–	–	30	26	-4	38	47	7.96	-108	-72.1
O3HP_FA_leaf_20210614_1830	0.3	0.010	27	24	-3	38	45	9.96	-135	-84.5
O3HP_FA_leaf_20210614_1945	0.5	0.021	24	22	-2	43	48	10.49	-151	-87.2
O3HP_FA_leaf_20210614_2135	0.4	0.016	21	20	-2	41	45	6.29	-110	-61.6
O3HP_FA_leaf_20210615_0315	0.1	0.013	15	16	1	97	92	3.86	-91	-44.4
O3HP_FA_leaf_20210615_0445	0.0	0.003	14	16	1	97	90	2.49	-85	-36.5
O3HP_FA_leaf_20210615_0615	0.7	0.087	19	20	1	91	87	2.12	-60	-31.2
O3HP_FA_leaf_20210615_0800	1.8	0.075	24	23	-1	69	74	2.55	-43	-31.2
O3HP_FA_leaf_20210615_0930	1.3	0.063	27	25	-2	67	75	2.31	-45	-27.2
O3HP_FA_leaf_20210615_1100	1.9	0.079	28	25	-3	58	70	4.60	-65	-42.5
O3HP_FA_leaf_20210615_1230	3.7	0.118	30	27	-3	51	58	5.10	-65	-44.7
O3HP_FA_leaf_20210615_1400	3.9	0.111	31	27	-4	43	53	4.22	-62	-40.4
O3HP_FA_leaf_20210615_1530	2.2	0.089	28	26	-2	63	69	4.32	-63	-39.2
O3HP_FA_leaf_20210615_1700	1.6	0.078	27	25	-2	63	72	4.94	-32	-46.4

https://doi.org/10.5194/bg-2022-230
Preprint. Discussion started: 9 December 2022

Table 2: Grass and phytolith descriptors, phytolith isotope composition, atmospheric temperature (T_{air}), plot-scale grass leaf temperature (T_{plot}), relative humidity (RH) and the ratio between actual atmospheric vapor pressure and saturation vapor pressure at T_{plot} (h) for the three regrowth periods. Grass height = grass height at the harvest day, LC = long cell vs short and long cell phytoliths ratio. Observed RH and h values are compared to estimated values using $^{17}O\text{-excess}_{phyto}$ and Eqs. (6)–(7), respectively (RH_{phyto} and h_{phyto}, respectively). SD = 1 standard deviation, $\Delta T_{leaf\text{-}air} = T_{plot}\text{-}T_{air}$.

Sample	spring	summer	autumn
Regrowth period	17/02/2021–20/05/2021	15/06/2021–27/08/2021	27/08/2021–23/11/2021
Grass and phytolith descriptors			
Grass height (cm)	43	25	18
Silicification rate (% SiO_2 dry weight d^{-1})	2.7	5.2	5.9
LC (%)	30	46	70
Phytolith isotope composition			
$\delta'^{18}O_{phyto}$ (‰)	36.6±0.2	35.9±0.5	34.3±0.6
$^{17}O\text{-excess}_{phyto}$ (per meg)	-256±2	-263±4	-234±3
Observed temperature and relative humidity parameters			
T_{air} daily (°C)	9±3	22±2	13±4
T_{air} daytime (°C)	12±3	24±3	16±4
T_{plot} daily (°C)	9±3	21±2	13±4
T_{plot} daytime (°C)	12±3	23±2	15±4
$\Delta T_{leaf\text{-}air}$ daily (°C)	-0.1±1.0	-0.6±0.6	-0.1±0.5
$\Delta T_{leaf\text{-}air}$ daytime (°C)	0.3±1.2	-1.1±0.8	-0.7±0.5
RH daily (%)	71±15	64±10	81±10
RH daytime (%)	62±17	57±11	73±12
h daily (%)	71±14	66±8	81±10
h daytime (%)	61±17	61±9	76±11
Estimated RH and h			
RH_{phyto} (%)	59	57	64
h_{phyto} (%)	66	64	71
Difference between estimated and observed RH and h			
RH_{phyto}-RH daily (%)	-12	-6	-17
RH_{phyto}-RH daytime (%)	-4	0	-9
h_{phyto}-h daily (%)	-5	-2	-10
h_{phyto}-h daytime (%)	5	3	-4

https://doi.org/10.5194/bg-2022-230
Preprint. Discussion started: 9 December 2022

2.3 Extractions and isotope analyses

2.3.1 Irrigation water, precipitation and atmospheric water vapor

A Picarro L2140-i CRDS, operated in ^{17}O Dual Liquid/Vapor mode was installed on-site for the experiment. The isotope composition and mixing ratio of water vapor in the air at 0.4 m above the grass plot was measured for 70 min every 140 min during the spring monitoring and every 280 min during the monitoring in summer and autumn. In between these measurements, the instrument was used for another experiment. The atmospheric water vapor data from the first 10 minutes of each measurement cycle were removed to account for memory effects and provide sufficient time to establish a stable baseline. The remaining 60 minutes were averaged. During the 24-hour monitoring, air sampling was performed continuously without interruption. Liquid water standard measurement runs were performed on a weekly basis. The mean of four measurement runs of liquid water standards was used to normalize the atmospheric water vapor isotope data to VSMOW-SLAP scale. The calibration protocol is described in detail by Voigt et al. (2022). In brief, three liquid water standards that covered the expected isotope range of atmospheric water vapor at the study site were analyzed at a water mixing ratio of 11000 ppmv using a Picarro autosampler system (A0325, Picarro Inc., California, US) coupled to a high-precision vaporizer (A0211, Picarro Inc., California, US). The liquid standards were injected in a dry air stream, produced by a lubricated mobile air compressor (MONTECARLO FC2, ABAC air compressors, Italy), further dried using two drierite columns combined with a dry ice trap (Voigt et al., 2022). Raw isotope compositions of the liquid standards of four consecutive measurement runs were averaged and then corrected to the water mixing ratio of the measured atmospheric water vapor, using the mean of three mixing ratio dependency functions that were determined on site for water mixing ratios between 3000 and 30000 ppmv in May 2021, October 2021 and January 2022 (Fig. A1). The precision of calibrated and integrated atmospheric water vapor data was determined using a Monte Carlo simulation (Voigt et al., 2022). Precision was better than ± 0.1 ‰, ± 0.2 ‰, ± 1.8 ‰ and ± 14 per meg, and ± 0.9 ‰ for $\delta^{17}O$, $\delta^{18}O$, $\delta^{2}H$, ^{17}O-excess, and d-excess, respectively.

A second Picarro L2140-i CRDS operated in ^{17}O-High Precision mode was used at CEREGE to analyze the isotope composition of irrigation water and precipitation. Isotope analyses, correction of memory effects and VSMOW-SLAP scaling were performed following Vallet-Coulomb et al. (2021). The external reproducibility of a quality control standard (1 standard deviation (SD), n = 12) measured along with the samples in each sequence was ± 0.02 ‰, ± 0.03 ‰, ± 0.3 ‰, ± 6 per meg, and ± 0.1 ‰ for $\delta^{17}O$, $\delta^{18}O$, $\delta^{2}H$, ^{17}O-excess, and d-excess, respectively.

2.3.2 Plant water

Plant water was extracted by cryogenic vacuum distillation (static pressure < 10 Pa) with sample vials placed in the vacuum line and immersed in a heated water bath for 3 h with a final target temperature set to 80 °C (attained within 45 min of extraction). A detailed description of the system design is given by Barbeta et al. (2022). Isotope analysis of plant waters was performed at the University of Cologne. For triple oxygen isotope analysis, pure O_2 liberated from plant waters by fluorination

https://doi.org/10.5194/bg-2022-230
Preprint. Discussion started: 9 December 2022

was introduced in a Thermo Fisher Scientific MAT 253 dual-inlet mass spectrometer (Massachusetts, USA), following the procedure described by Surma et al. (2015). The reproducibility (1 SD, n = 2) of $\delta^{17}O$, $\delta^{18}O$ and ^{17}O-excess measurements was better than ± 0.15 ‰, ± 0.30 ‰ and ± 11 per meg, respectively. Hydrogen isotope ratios were determined by high-temperature carbon reduction in a pyrolysis elemental analyzer (HEKAtech GmbH, Wegberg, Germany), coupled to the mass spectrometer. The reproducibility (1 SD, n = 3) of δ^2H measurements was always better than 1.1‰. An intercomparison of water analysis at CEREGE and the University of Cologne was performed. The results are presented in Table S1. Differences between the laboratories were lower than 0.2 ‰, 0.3 ‰, 1.1 ‰, 14 per meg, and 1.6 ‰ for $\delta^{17}O$, $\delta^{18}O$, δ^2H, ^{17}O-excess, and d-excess, respectively. Similar differences were found in an intercomparison between the two Picarro CRDS instruments (Alexandre et al., 2018).

2.3.3 Phytoliths

The silica contents of harvested grass blades were determined by inductively coupled plasma-atomic emission spectroscopy (Ultima C, Horiba Jobin Yvon, Longjumeau, France). Phytoliths were extracted following the protocol detailed in Corbineau et al. (2013). The phytoliths were mounted on microscope slides in Canada Balsam and different types were counted using light microscopy at a 600X magnification. The epidermal silicified intercoastal long cells were quantified relative to the silicified short cells to obtain information on the silicification process (Alexandre et al., 2019).

The phytolith samples (1.6 mg) were dehydrated at 1100 °C under a flow of N_2 (Chapligin et al., 2010) to prevent the formation of siloxane from silanol groups during dehydroxylation. Molecular O_2 was extracted using the IR laser-heating fluorination technique (Alexandre et al., 2006; Crespin et al., 2008; Outrequin et al., 2021). At the end of the procedure, the gas was passed through a -114 °C slush to refreeze any molecule interfering with the mass 33 (e.g., NF potentially remaining in the line). The gas was directly sent to a ThermoQuest Finnigan Delta V Plus dual-inlet mass spectrometer (Massachusetts, USA) for triple oxygen isotope analysis. Each gas sample was run twice with each run consisting of eight dual-inlet cycles. A third run was performed when the standard deviation on the first two averages was higher than 12 per meg for ^{17}O-excess. The reproducibility for $\delta^{18}O$ and ^{17}O-excess measurements of the quartz laboratory standard was 0.16 ‰ and 8 per meg, respectively (1 SD, n = 5). For the phytolith samples the precision for $\delta^{18}O$ and ^{17}O-excess was better than 0.5 ‰, and 12 per meg (1 SD), respectively. The sample measurements were corrected using a quartz laboratory standard analyzed at the beginning of the day until a ^{17}O-excess plateau was reached and again at the end of the day. The isotope composition of the reference gas was determined against NBS28. For robust comparisons between silica and water isotope compositions, the phytolith data are normalized to VSMOW-SLAP scale (Outrequin et al., 2021).

2.4 Modelling

The isotope fractionation during water vapor diffusion in air through the leaf stomata and boundary layer (α_{diff}) was estimated as:

https://doi.org/10.5194/bg-2022-230
Preprint. Discussion started: 9 December 2022

$$\alpha_{diff} = \frac{\alpha_{kin}/g_s + {\alpha_{kin}}^{2/3} g_b}{1/g_s + 1/g_b} \quad (4)$$

where g_s and g_b (mol m^{-2} s^{-1}) denote the stomatal and leaf boundary layer conductances, and α_{kin} denotes the kinetic fractionation during molecular diffusion of water vapor in air. We took $^{18}\alpha_{kin}$ = 1.028 and $^{2}\alpha_{kin}$ = 1.025 from Merlivat et al. (1978) for $^{18}O/^{16}O$ and $^{2}H/^{1}H$, respectively. For equilibrium fractionation between water and water vapor, temperature-dependent fractionation factors (α_{eq}) for $^{18}O/^{16}O$ and $^{2}H/^{1}H$ reported by Majoube et al. (1971) are used herein. The fractionation factors for $^{17}O/^{16}O$ are derived from those of $^{18}O/^{16}O$ according to $^{17}\alpha = {}^{18}\alpha^{\theta}$ using θ_{eq} = 0.529 for liquid-vapor equilibrium (Barkan and Luz, 2005) and θ_{kin} = 0.5185 for the kinetic fractionation during molecular diffusion (Barkan and Luz, 2007).

The fraction of the unevaporated leaf water pool (*f*) was set to 0.2. Similar values were obtained in previous studies (Wang et al., 2018; Alexandre et al., 2019; Hirl et al., 2019). Hirl et al. (2019) found no evidence of a dependency of *f* on the transpiration rate of grasses from a mixed grassland. Therefore, this effect was not accounted for in our study.

As leaf water can deviate from isotope steady state, non-steady state enrichment of leaf water was modelled for the 24-hour monitoring, using the following equation (Dongmann et al., 1974; Farquhar and Cernusak, 2005; Hirl et al., 2019):

$$R_{leaf}(t_0 + \Delta t) = R_{leaf,ss}(t_0 + \Delta t) + (R_{leaf}(t_0) - R_{leaf,ss}(t_0 + \Delta t)e^{-\frac{\Delta t}{\tau}}, \quad (5a)$$

With $$\tau = \frac{W \alpha_{eq} \alpha_{diff}}{g w_i} \quad (5b)$$

where $g = g_s\, g_b/(g_s+g_b)$, w_i is the mole fraction of water vapor in air in the intercellular spaces, *W* is the leaf water content and $R_{leaf,ss}$ denotes the isotope composition of bulk leaf water at steady state, as predicted by Eq. (2). Compared to Farquhar & Cernusak (2005) or Hirl et al. (2019), we neglected diurnal changes in *W*, which should result in only ~ 3 % error in predicted leaf water isotope enrichment (Farquhar and Cernusak, 2005). We set *W* to a value of 6 mol m^{-2}, adjusted to the observed leaf water isotope composition.

3 Results

3.1 Changes in the isotope composition of atmospheric water vapor, precipitation, and irrigation water

Over the experimental period, the isotope composition of irrigation water that mainly fed the soil water, was stable, averaging -7.4 ± 0.2 ‰ for $\delta^{18}O$, -48.5 ± 0.7 ‰ for $\delta^{2}H$, 10.7 ± 0.6 ‰ for d-excess and 31 ± 6 per meg for ^{17}O-excess (Fig. A2). These values are close to the amount-weighted annual averages of precipitation in 2021: -8.1 ± 2.9 ‰ for $\delta^{18}O$, -52 ± 24 ‰ for $\delta^{2}H$, 12.0 ± 3.5 ‰ for d-excess and 29 ± 11 per meg for ^{17}O-excess (Table S2). The precipitation (730 mm a^{-1}) was mainly distributed between two periods in spring (April to May) and autumn (October to December) (Fig. 1, Table S2).

https://doi.org/10.5194/bg-2022-230
Preprint. Discussion started: 9 December 2022

The annual average isotope composition of atmospheric water vapor was -17.4 ± 3.1 ‰ for $\delta^{18}O$, -126 ± 24 ‰ for $\delta^{2}H$, 13.0 ± 1.7 ‰ for d-excess and 28 ± 5 per meg for ^{17}O-excess. These values coincide with $\delta^{18}O$, $\delta^{2}H$, d-excess and ^{17}O-excess values estimated for a water vapor in isotope equilibrium with the amount-weighted precipitation (Table S2). As for precipitation, the atmospheric water vapor monthly averages in $\delta^{18}O$ and $\delta^{2}H$ increase from winter to summer, whereas averages in d-excess and ^{17}O -excess decrease (Fig. 1; Table S2). During the 24-hour monitoring, $\delta^{18}O$ of atmospheric water vapor increased overnight from about -16 to -12‰ and then stabilized. The d-excess and ^{17}O-excess of atmospheric water vapor showed diurnal variations, reaching respective minimum values of -3.2 ‰ and -10 per meg in the early morning and respective maximum values of 18.4 ‰ and 36 per meg at noon (Table S3).

https://doi.org/10.5194/bg-2022-230
Preprint. Discussion started: 9 December 2022

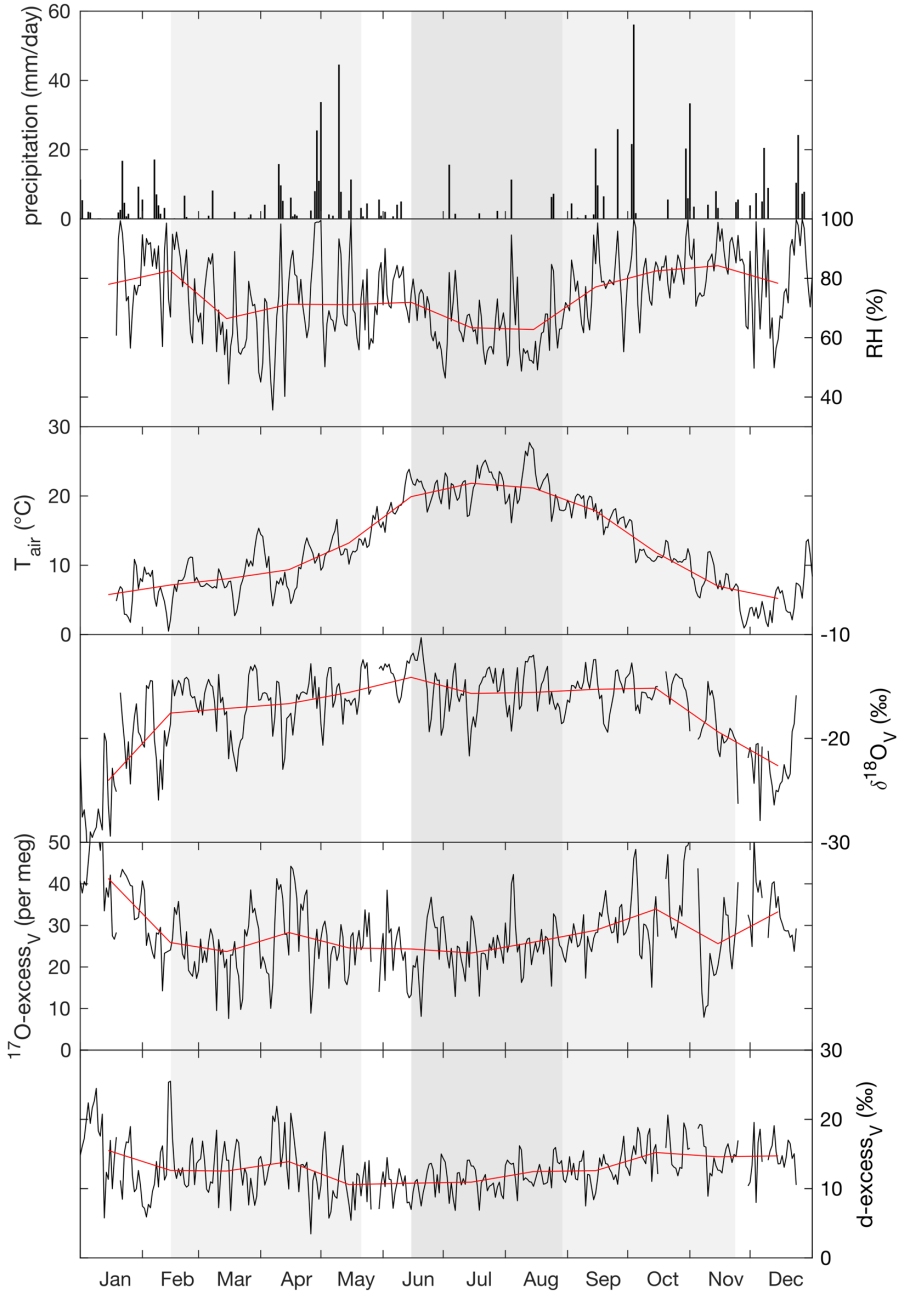

Figure 1: Daily precipitation amount, daily (black) and monthly (red) means of relative humidity (RH) and atmospheric temperature (T_{air}) measured at 60 cm above the ground next to the grass plot, and the isotope composition of atmospheric water vapor ($\delta^{18}O_V$, $^{17}O\text{-excess}_V$, $d\text{-excess}_V$) measured at 40 cm height above the grass plot monitored at the O_3HP platform from February to November 2021. The three regrowth periods lasting from 17 February–20 May 2021 (spring), from 15 June–27 August 2021 (summer) and from 27 August–23 November 2021 (autumn) are indicated by shaded areas.

https://doi.org/10.5194/bg-2022-230
Preprint. Discussion started: 9 December 2022


Biogeosciences Discussions Open Access EGU

3.2 Changes in RH, temperature, stomatal conductance, transpiration and the isotope composition of grass leaf water

Table 1 and Figure 2 show changes in RH, h, T_{air}, T_{plot}, *F. arundinacea* leaf transpiration and stomatal conductance averaged over 30 minutes before the 8 grass leaf samplings at midday. RH is always equal or lower than h (by less than 9 %) but co-varies with h from low values in spring and summer (30–40 %) to high values in autumn (ca. 64 %). T_{plot} is 1–3 ºC lower than T_{air} but changes along with T_{air} from a measurement day to another, with high values in summer (ca. 25 °C), and lower values in spring (ca. 18 °C) and autumn (ca. 14 °C). Figure A3 shows five daily variations of T_{air}, T_{plot} and T_{leaf}. Although T_{leaf} varies spatially within the plot, its spatial average around midday is close to T_{plot} (Fig. A3), supporting that T_{plot} can be considered as an approximation of T_{leaf}. Transpiration and stomatal conductance are relatively stable from a measurement day to another, varying from 1.1–3.7 mol m^{-2} s^{-1} and 0.05–0.13 mol m^{-2} s^{-1}, respectively (Fig. 2).

The isotope composition of *F. arundinacea* leaf water sampled at midday is also shown in Table 1 and Figure 2. The leaf water has $\delta^{18}O$ (-0.05 ‰ to 20.1 ‰) and $\delta^{2}H$ (-31 ‰ to 18 ‰) that are higher than irrigation water, and d-excess (-31.0 ‰ to -142.8 ‰) and ^{17}O-excess (17 per meg to -165 per meg) that are lower than irrigation water, as can be expected for an evaporation signal. The changes in $\delta^{18}O$, $\delta^{2}H$, d-excess and ^{17}O-excess observed from a sampling day to another follow the changes in RH and h (Fig. 2). Evaporative isotope enrichment is highest in May and July, when RH is low and lowest in November when RH is high. Samples from October and November have similar d-excess as expected from little variation in RH (64 ± 2 %). However, their ^{17}O-excess values differ by ca. 65 per meg. The reason for this difference in ^{17}O-excess remains unclear.

Table 1 and Figure 3 show the 24-hour evolution of the isotope composition of leaf water from 14–15 June 2021 in relation to RH, h, T_{air}, T_{plot}, transpiration and stomatal conductance. T_{air} and RH range from 14 °C to 31 °C and 38 % to 97 %, respectively. T_{plot} is ca. 1 °C higher than T_{air} at night, and up to 4 °C lower than T_{air} during daytime. During daytime, stomatal conductance measured continuously on a single leaf, ranges from 0.06 mol m^{-2} s^{-1} to 0.12 mol m^{-2} s^{-1} and co-varies with transpiration (1.3 to 3.9 mol m^{-2} s^{-1}). However, stomatal conductance varies greatly (by 0.20 mol m^{-2} s^{-1} to 0.50 mol m^{-2} s^{-1}) between different leaves in the grass plot (Fig. A4). At night, stomatal conductance is never higher than 0.02 mol m^{-2} s^{-1}, while transpiration remains lower than 0.5 mol m^{-2} s^{-1}. The isotope variability of leaf water on this diurnal scale is of the same order of magnitude as the changes observed among samples collected at midday in different months. The evolution of the isotope composition of leaf water follows RH and h, except for samples collected at night and in the early morning when transpiration is low. During this time, stomatal closure impeded exchange between the leaf and the atmosphere, decoupling the isotope composition of leaf water from RH.

https://doi.org/10.5194/bg-2022-230
Preprint. Discussion started: 9 December 2022

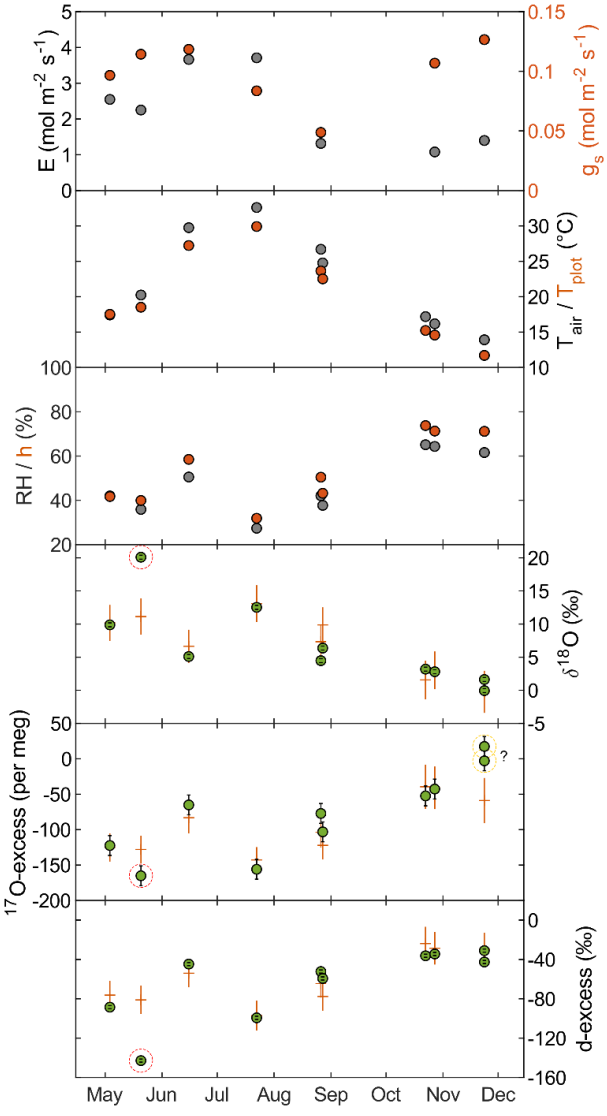

Figure 2: Transpiration (E), stomatal conductance (g_s), atmospheric temperature (T_{air}), plot-scale grass leaf temperature (T_{plot}), relative humidity (RH), water vapor pressure ratio between leaf and the atmosphere (h), and measured (circles) and predicted (+) isotope composition of *F. arundinaceae* leaf water ($\delta^{18}O$, ^{17}O-excess, d-excess) for midday samples over the year 2021 (see Table 1 for sampling dates). Error bars of isotope data represent analytical precision (see method section). The modeled isotope composition of bulk leaf water is predicted by the C-G model (Eqs. (1), (2)) using average environmental conditions over 30 minutes before sampling (Table 1, S3). The model uncertainty (1 SD) was estimated using a Monte Carlo simulation accounting for uncertainty of input variables (RH ± 1 %, T_{plot} ± 2 °C, $\delta^{18}O_S$ ± 0.2 ‰, d-excess$_S$ ± 0.6 ‰, ^{17}O-excess$_S$ ± 6 per meg, $\delta^{18}O_V$ ± 0.2 ‰, d-excess$_V$ ± 0.9 ‰, ^{17}O-excess$_V$ ± 14 per meg, g_s ± 0.1 mol m^{-2} s^{-1}, and the fraction of unevaporated water pools (*f*) ± 0.1). Dashed circles indicate the sample that has been likely affected by evaporation during sampling (red) and samples with anomalously high ^{17}O-excess relative to d-excess (yellow).

https://doi.org/10.5194/bg-2022-230
Preprint. Discussion started: 9 December 2022

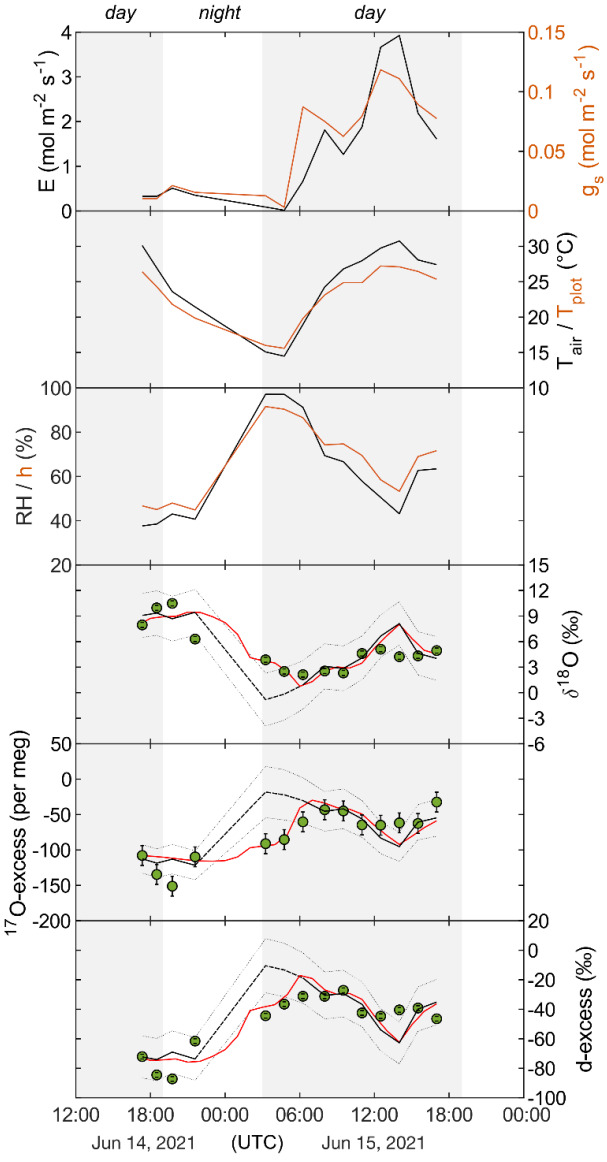

Figure 3: 24-hour monitoring of transpiration (E), stomatal conductance (g_s) atmospheric temperature (T_{air}), plot-scale grass leaf temperature (T_{plot}), relative humidity (RH), water vapor pressure ratio between leaf and the atmosphere (h), and the observed (circles) and predicted steady state (black curve, Eq. (2)) and non-steady state (red curve, Eq. (5)) isotope composition of *F. arundinaceae* leaf water ($\delta^{18}O$, ^{17}O-excess, d-excess) from 14–15 June 2021. Error bars of isotope data represent analytical precision (see method section). Shaded areas mark daytime interval. The isotope composition of leaf water is predicted using average environmental conditions over 30 minutes before sampling (Table 1, S3, S4). The pointed lines represent model uncertainty (1 SD) of the C-G model prediction estimated using a Monte Carlo simulation (see caption Figure 2). The dashed part of the steady state prediction represents the time when leaf water isotope composition deviates from steady-state due to low transpiration and long leaf water residence times (see discussion for details).

https://doi.org/10.5194/bg-2022-230
Preprint. Discussion started: 9 December 2022


Biogeosciences Discussions Open Access EGU

335 **3.2.1 Model-data comparison**

For six of eight midday sampling days, the isotope composition of bulk leaf water predicted by the C-G model (Eq. (2)) using boundary conditions averaged over 30 minutes before sampling (Table S3) agrees with the measured isotope values within model uncertainty, that is in average ± 2.7 ‰, ± 15 ‰, and ± 25 per meg for $\delta^{18}O$, d-excess and ^{17}O-excess, respectively (Fig. 2). Samples collected on 20 May 2021 and 23 November 2021 show larger discrepancies between observed and predicted
340 values. The May sample has significantly higher $\delta^{18}O$ (> 8 ‰) and lower d-excess (59 ‰) and ^{17}O-excess (33 per meg) than respective steady state values predicted by the C-G model (Fig 2). These large deviations are indicative of significantly stronger evaporation than expected. In view of the large magnitude of the deviation, we suppose that the sample was affected by evaporation during sampling. We therefore exclude this sample from further discussion. For the November sample, $\delta^{18}O$ and d-excess agree within 1.1 ‰ and 8 ‰ with the predicted steady state values, respectively. However, the ^{17}O-excess is
345 66 per meg higher than the predicted steady state value (Fig. 2). The reason for this discrepancy remains unclear.

For the 24-hour monitoring, the steady-state C-G model combined with the two-pool mixing equation (Eq. (2)) reproduces the evolution of the isotope composition of leaf water during the day, but not at night and in the early morning, when stomatal conductance and transpiration are low (Fig. 3). During daytime, best agreement between predicted and observed leaf water is found for samples collected on the morning of 15 June 2021 until midday, with deviations lower than ± 0.6 ‰ for $\delta^{18}O$, ± 6 ‰
350 for d-excess and ± 8 per meg for ^{17}O-excess. However, on the afternoon of 15 June 2021, when transpiration is highest, observed $\delta^{18}O$ are 1.5–4 ‰ lower and d-excess and ^{17}O-excess are 9 ‰ and 34 per meg lower than predicted values, respectively. In contrast, on the evening of 14 June 2021, observed $\delta^{18}O$ are 1–2 ‰ higher, whereas d-excess and ^{17}O-excess are respectively 18 ‰, and 38 per meg lower than respective steady state values predicted by the C-G model. The non-steady-state equation (Eq. (5)) was applied for night predictions to match the data (Fig. 3). Differences between predicted non-steady
355 state and observed values at night range from 0.2–3.6 ‰ for $\delta^{18}O$, 3–19 ‰ for d-excess and 1–31 per meg for ^{17}O-excess (Table S4). Note that a leaf water content of 6 mol m^{-2} is required for the model to fit the data (Table S4). This value is higher than leaf water contents reported for grasses in previous studies (2–4 mol m^{-2}; Hirl et al., 2019; Barbour et al., 2021).

3.2.2 Sensitivity tests

Figure 4 shows for the 24-hour monitoring the uncertainty of the bulk leaf water isotope composition predicted for steady state
360 conditions (Eq. (2)) introduced by the precisions associated with the measurement of the main model parameters. A ± 5 % uncertainty on RH introduces an uncertainty of ± 1.5 ‰ on $\delta^{18}O$, ± 4.0 ‰ on $\delta^{2}H$, ± 10‰ on d-excess, and ± 13 per meg on ^{17}O-excess of leaf water. For an RH range of 40–80 %, an uncertainty of ± 0.1 on the fraction of the unevaporated water pool (*f*) leads to an uncertainty of 2.2–0.8 ‰ on $\delta^{18}O$, 6–2 ‰ on $\delta^{2}H$, 12–4 ‰ on d-excess and 16–6 per meg on ^{17}O-excess. For the same RH range, misestimation of $T_{leaf\text{-}air}$ by 2 °C leads to an uncertainty of 1.3–2.7 ‰ on $\delta^{18}O$, 1.5–5.1 ‰ on $\delta^{2}H$, 9–17 ‰
365 on d-excess and 11–29 per meg on ^{17}O-excess. Assuming T_{leaf} equals T_{air}, instead of measuring T_{plot}, increases the difference

https://doi.org/10.5194/bg-2022-230
Preprint. Discussion started: 9 December 2022

between the predicted and observed daytime $\delta^{18}O$, $\delta^{2}H$, d-excess and ^{17}O-excess values by 1.1 ± 1.2 ‰, 2.4 ± 0.5 ‰, 5 ± 11 ‰ and 10 ± 14 per meg, respectively. By contrast, assuming T_{leaf} is 2 °C lower than T_{air}, only slightly increases the difference between predicted and observed daytime $\delta^{18}O$, $\delta^{2}H$, d-excess and ^{17}O-excess values by 0.2 ± 0.6 ‰, 3.0 ± 5.5 ‰, 2 ± 4 ‰ and 3 ± 5 per meg, respectively. In contrast to RH, *f* and the $\Delta T_{leaf\text{-}air}$, measurement uncertainties on the isotope composition of the source water (irrigation water) and atmospheric water vapor, introduce uncertainties on the isotope composition of leaf water that are close to or lower than analytical precision. Using the isotope composition of atmospheric water vapor estimated from isotope equilibrium with the mean annual amount-weighted O_3HP precipitation (Table 2) instead of measured values, increases the difference between predicted and observed daytime $\delta^{18}O$, $\delta^{2}H$, d-excess and ^{17}O-excess values by 1.2 ± 2.0 ‰, 12.5 ± 12.3 ‰, 0 ± 2 ‰ and 3 ± 8 per meg, respectively. Observed spatial variability of stomatal conductance of up to 0.50 mol m^{-2} s^{-1} introduces a bias on the $\delta^{18}O$, $\delta^{2}H$, d-excess and ^{17}O-excess of less than 0.5 ‰, 0.5 ‰, 3.5 ‰ and 10 per meg, respectively.

https://doi.org/10.5194/bg-2022-230
Preprint. Discussion started: 9 December 2022

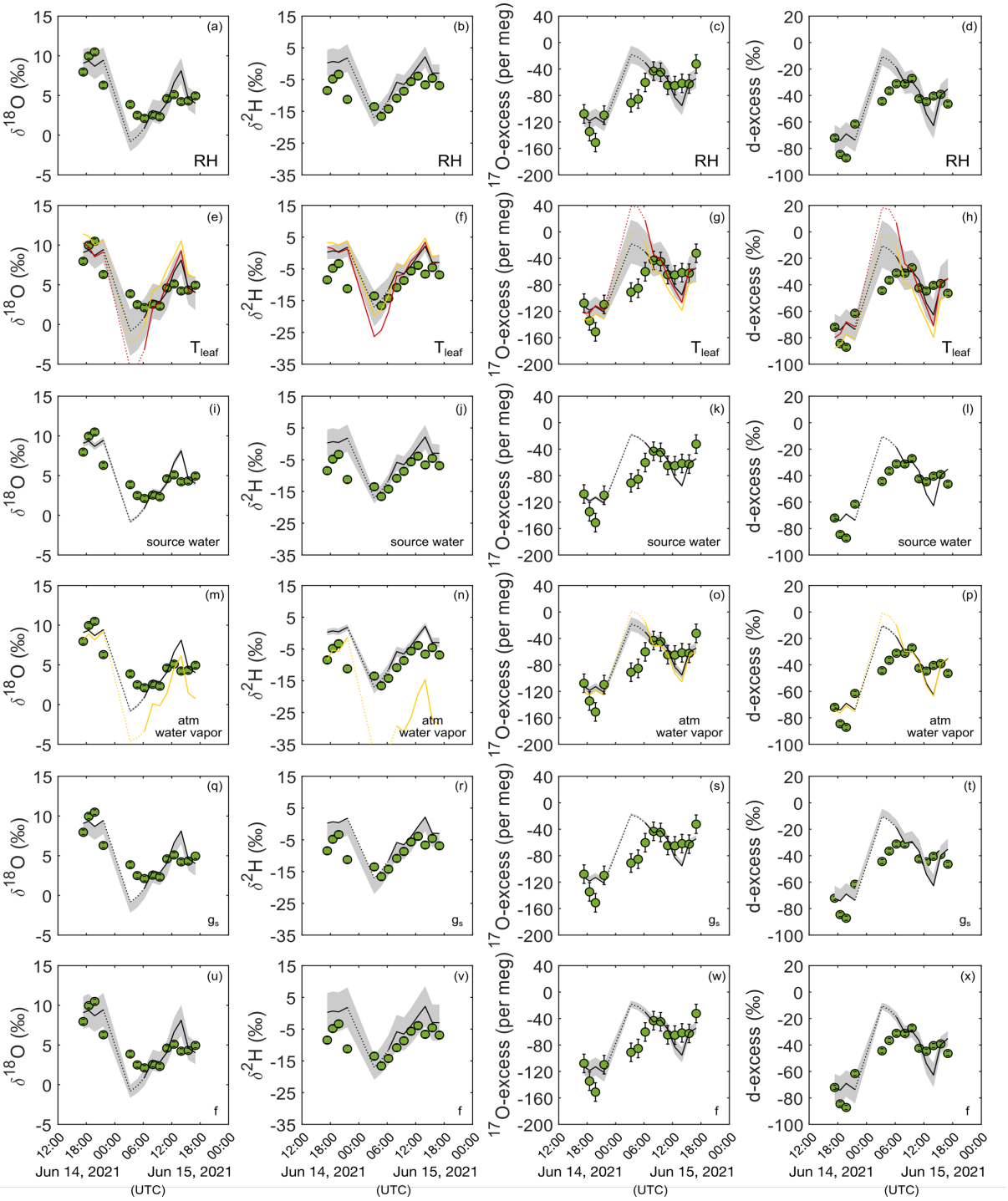

https://doi.org/10.5194/bg-2022-230
Preprint. Discussion started: 9 December 2022

Figure 4: Sensitivity of $\delta^{18}O$, $\delta^{2}H$, ^{17}O-excess and d-excess of leaf water to changes in environmental and plant physiological parameters. Green circles represent measured *F. arundinaceae* leaf water isotope composition over a 24-hour period from 14–15 June 2021. The black line shows the steady state leaf water isotope composition predicted by the C-G model using mean boundary conditions over 30 minutes before sampling (Table 1). Shaded areas indicate the sensitivity of the predicted leaf water isotope composition for relative humidity (RH) (± 5 %) (a–d), leaf temperature (T_{leaf}) (± 2 °C) (e–h), the isotope composition of source water (± 0.2 ‰ for $\delta^{18}O_S$, ± 0.7 ‰ for $\delta^{2}H_S$, ± 0.6 ‰ for d-excess$_S$, ± 6 per meg for ^{17}O-excess$_S$) (i–l), the isotope composition of atmospheric water vapor (± 0.2 ‰ for $\delta^{18}O_V$, ± 1.8 ‰ for $\delta^{2}H_V$, ± 0.9 ‰ for d-excess$_V$, ± 14 per meg for ^{17}O-excess$_V$) (m–p) stomatal conductance (g_s) (± 0.1 mol m^{-2} s^{-1}) (q–t), and the fraction of unevaporated water pools (*f*) (± 0.1) (u–x). Coloured curves show the isotope composition of leaf water predicted by the C-G model (Eq. (2)) (i) when assuming leaf temperatures being equal to atmospheric temperature (panel e–h, yellow), (ii) when assuming leaf temperatures being 2 °C lower than atmospheric temperature (panel e–h, red), and (iii) when estimating atmospheric water vapor from isotope equilibrium with source water (irrigation water) (panel m–p, yellow).

3.3 Changes in climate averages, grass height, silicification rate, and triple oxygen isotope composition of phytolith assemblages

Table 2 shows daily and daytime climate averages, maximum grass height, silicification rate, ratio of long cell to short and long cell phytoliths, and triple oxygen isotope composition of phytoliths for the three regrowth periods. T_{air} daily average is from 9 °C to 22 °C and RH daily average is from 64 % to 81 %. T_{air} daytime average is about 2.4 °C higher than the daily average. RH daytime average is about 8 % lower than the daily average. Daily averages of T_{plot} are similar to T_{air}, so that RH approximates h (cf. section 2.4). During daytime, averages of RH and h differ by 1–4 % due to the $\Delta T_{leaf\text{-}air}$ of -1.1 °C to 0.3 °C. Daytime h average is 61 % in spring and summer, and 76 % in autumn. The average soil water content is always higher than 0.20 ± 0.05 L L^{-1}, whatever the regrowth, supporting that the grass plot is always well-watered, and that water stress is excluded.

Grass height increases exponentially during spring regrowth, and linearly during summer regrowth (Fig. A5). During the autumn regrowth, the grass height increases only in the first month of the regrowth and stabilizes thereafter (Fig. A5). The silicification rate (from 2.7 to 5.9 SiO_2 g^{-1} d^{-1}), and the ratio of long cell to short and long cell phytoliths (from 30 to 70 %) increase with the number of regrowth periods, without any correlation with RH or h that varied little from a regrowth to another (Table 2). The $\delta'^{18}O$ and ^{17}O-excess of the grass leaf phytoliths are similar in spring and summer (36.2 ± 0.5 ‰ and -260 ± 5 per meg, respectively; Table 2) and slightly different in autumn (34.3 ‰ and -234 per meg, respectively). The high silicification rate and high ratio of long cell to short and long cell phytoliths obtained for the third regrowth phytolith assemblage can thus be explained by more time allocated to the grass leaf at maturity for epidermal long cell silicification (Motomura et al., 2004). It was previously shown that the ratio of long cell to short and long cell phytoliths changes with RH and grass leaf development stage (Alexandre et al., 2018, 2019). Here, the effect of RH on the phytolith ratio is masked by the effect of the leaf development stage.

https://doi.org/10.5194/bg-2022-230
Preprint. Discussion started: 9 December 2022

Biogeosciences Discussions Open Access EGU

3.4 Relationship between the ^{17}O-excess of phytoliths and leaf water

The isotope composition of phytoliths is used to reconstruct the isotope composition of their forming water using the fractionation coefficients $^{18}\alpha_{phyto\text{-}H2O}$ and $\lambda_{phyto\text{-}H2O}$. $^{18}\alpha_{phyto\text{-}H2O}$ can be calculated from the temperature-dependent equation obtained by Dodd and Sharp (2010) or Sharp et al. (2016). $\lambda_{phyto\text{-}H2O}$ can be set at 0.522, which is the apparent $\lambda_{phyto\text{-}H2O}$ value systematically obtained in phytolith studies (Outrequin et al., 2021) or 0.524 which is the value expected for equilibrium (Sharp et al., 2016). Using $\lambda_{phyto\text{-}H2O}$ of 0.522, the calculated isotope compositions of phytolith-forming water agree with the isotope compositions of leaf water predicted by the C-G model under daytime average climate conditions of the three regrowths (Fig. 5). The differences are lower than 1.7 ‰ and 10 per meg for δ'^{18}O and ^{17}O-excess, respectively. There is no agreement when a $\lambda_{phyto\text{-}H2O}$ value of 0.524 is considered (Fig. 5).

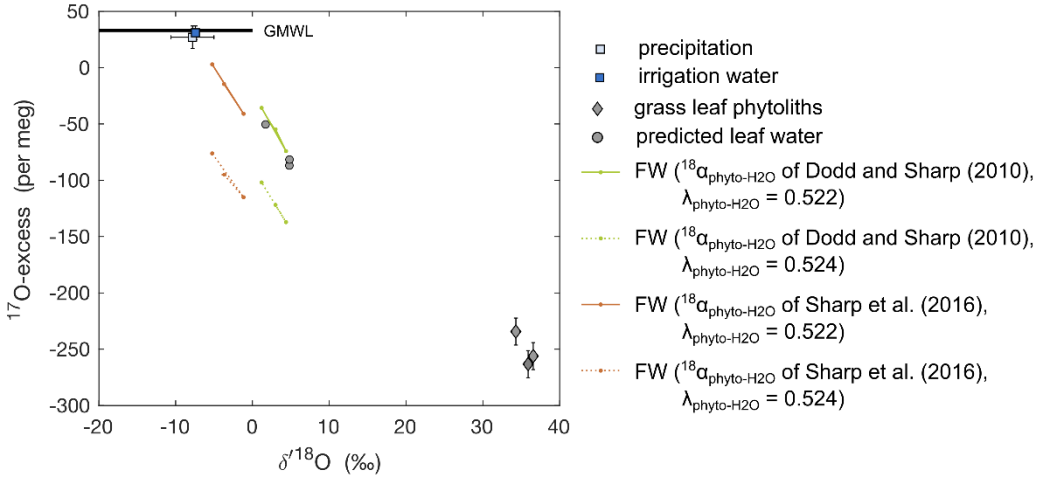

Figure 5: ^{17}O-excess vs δ'^{18}O of amount-weighted annual average precipitation, average irrigation water, and the isotope composition of phytoliths extracted from *F. arundinaceae* grass leaves harvested on 20 May 2021 (spring), 27 August 2021 (summer), and 23 November 2021 (autumn). Also shown are the formation water (FW) predicted using temperature-dependent equilibrium $^{18}\alpha_{SiO2\text{-}H2O}$ from Dodd and Sharp (2010) or Sharp et al. (2016) and $\lambda_{phyto\text{-}H2O}$ of 0.522 or 0.524, and the isotope composition of bulk leaf water predicted by the C-G model for steady state conditions (Eq. (2)) using average daytime boundary conditions for the three regrowth periods (Table 2). Error bars represent analytical precisions (see methods section), except for precipitation, for which the amount-weighted standard deviation is indicated.

4 Discussion

4.1 Parameters responsible for discrepancies between observed and predicted isotope compositions of grass leaf water

Overall agreement between the observed and predicted leaf water δ^{18}O and ^{17}O-excess trends from a sampling day to another shows that the C-G steady-state model combined with the two-pool mixing equation (Eqs. (1), (2)) is appropriate for estimating

https://doi.org/10.5194/bg-2022-230
Preprint. Discussion started: 9 December 2022

seasonal scale variations in the triple oxygen isotope composition of grass leaf water at midday. At the diurnal scale, the steady state C-G model reproduces correctly the trends in triple oxygen isotope evolution of leaf water during daytime although observed and predicted values diverge little when transpiration is maximal in the early afternoon (Fig. 3). As shown by the sensitivity tests, $\Delta T_{air\text{-}leaf}$ contributes largely to model uncertainty (Fig. 4). Assumptions on T_{leaf} equal to T_{air} can explain the discrepancies between predicted and observed isotope values often reported in the literature. In the present case, T_{leaf} was indirectly measured using T_{plot} and large misestimation of T_{leaf} (>2 °C) is unlikely. Part of the small model-data discrepancies in the afternoon on 15 June 2021 can result from RH measured at 60 cm above the ground next to the grass plot being lower than RH surrounding the grass leaf canopy, due to intense soil evaporation. Another bias may come from misestimation of the unevaporated water pool *f* that can drive large variations in the triple oxygen isotope composition of leaf water, as shown by the sensitivity tests. The value of 0.2 chosen for *f* in the present study is at the lower limit of previously reported values selected for grass species (0.2–0.4; Hirl et al., 2019; Barbour et al., 2021). Considering a value for *f* of 0.4 instead of 0.2 would minimize the discrepancy between observed and predicted $\delta^{18}O$ of leaf water for the samples taken in the afternoon on 15 June 2021 (Fig. 4). Some studies suggested that *f* may increase with increasing transpiration, due to increased advection of unevaporated xylem water, known as the Péclet effect (Farquhar and Lloyd, 1993; Cuntz et al., 2007). However, evidence for this effect is debated, and at least seems to be species dependent. The data from the 24-hour monitoring show a significant positive correlation ($R^2 = 0.49$) between transpiration and the difference between observed and predicted $\delta^{18}O$ values of leaf water. This is in contrast with recent leaf water isotope studies using different grass species that failed to detect a Péclet effect, even under water stress (Hirl et al., 2019). The Péclet effect that is not accounted for in our model approach can thus explain that predicted variations of the triple oxygen isotope composition of leaf water are larger than the observed ones when transpiration is high.

In agreement with previous studies on $\delta^{18}O$ and $\delta^{2}H$ (Farquhar and Cernusak, 2005; Cernusak et al., 2016), a non-steady state model is used to reproduce the trends in isotope evolution of leaf water at night when stomatal conductance and transpiration are low. Our results confirm the applicability of this model for the triple oxygen isotope composition of leaf water. In addition, the model-data comparison shows the advantage of ^{17}O-excess over d-excess in detecting non-steady state conditions in leaf water transpiration on a diurnal scale. Figure 6a illustrates the ^{17}O-excess vs $\delta'^{18}O$ evolution of leaf water from the beginning to the end of the night, when transpiration is too low to reach the steady state. RH of 96 ± 2% persisting between 3:00 and 7:00 (LT) on 15 June 2021 drives the theoretic steady state values to the upper end of the predicted trend on Fig. 6a. However, due to the long leaf water residence time, the observed leaf water isotope composition evolves only slowly towards these values without reaching them. This is well captured by the concave curvature of the non-steady state prediction (Fig. 6a). In contrast, linearity of evaporation trends in the d-excess vs $\delta^{18}O$ space challenges the differentiation between steady-state and non-steady-state conditions, as illustrated in Figure 6b.

https://doi.org/10.5194/bg-2022-230
Preprint. Discussion started: 9 December 2022

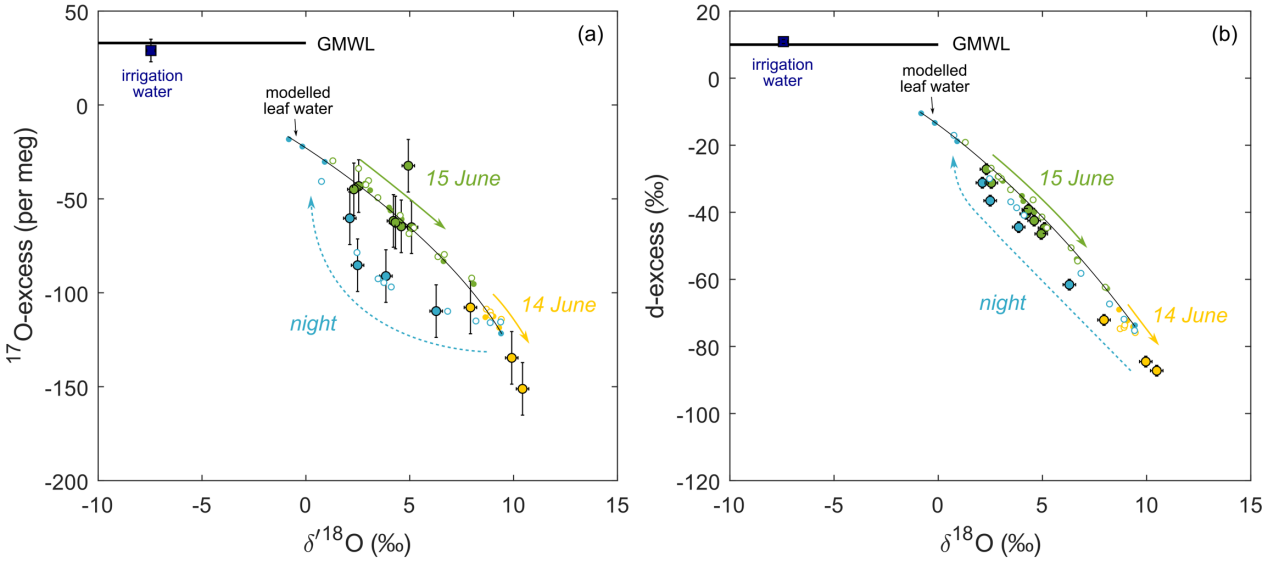

Figure 6: Comparison of predicted (small circles) and observed (large circles) *F. arundinacea* leaf water over a 24-hour period from 14–15 June 2021 in diagrams of (a) ^{17}O-excess vs δ'^{18}O and (b) d-excess vs δ^{18}O. Filled cycles indicate steady state model prediction (Eq. (2), Table S3), open cycles indicate non-steady state model prediction (Eq. (5), Table S4). Colours differentiate samples collected between 19:15 and 21:45 (LT) on 14 June 2021 (yellow), between 14 June 2021 23:30 and 15 June 2021 08:15 (LT) (blue) and between 10:00 and 19:00 on 15 June 2021 (green). The black line serves as a guide-of-the-eye for the trend in modelled isotope steady-state values. The average isotope composition of the irrigation water over the experimental period is also shown. The global meteoric water line (GMWL) is shown for comparison.

4.2. What can we learn from measurements of T_{plot} and triple oxygen isotope composition of atmospheric water vapor?

The sensitivity tests highlight the importance of two parameters that are difficult to measure, plot-scale grass leaf temperature and the isotope composition of atmospheric water vapor, on the isotope composition of leaf water.

Accurate measurements of T_{leaf} on plot-scale is challenging, as T_{leaf} can vary considerably in space and time, particularly according to soil moisture, leaf transpiration, canopy structure and position, net radiation, elevation and latitude (Still et al., 2019). Sufficient soil moisture supports transpiration, which generally leads to leaf cooling, i.e. T_{leaf} lower than T_{air}. On the contrary, water stress is compensated by stomata closure, which stops transpiration and increases T_{leaf}. In this case, T_{leaf} may exceed T_{air}, as demonstrated for irrigated *vs* rain-fed crops (Siebert et al., 2014). The amplitude of $\Delta T_{leaf\text{-}air}$ also increases with leaf size (Leuzinger and Körner, 2007). $\Delta T_{leaf\text{-}air}$ lower or equivalent to 2 °C was reported, at the ecosystem scale, for tropical forests (Rey-Sánchez et al., 2016), grasslands or cold desert areas, whereas larger differences were reported for cold forests and warm desert areas (Blonder and Michaletz, 2018). In the present case, continuous irrigation of the grass plot sustained the transpiration, leading to a daytime T_{leaf} consistently near or below the daytime T_{air} (Figs. A3, A6). However, under natural

https://doi.org/10.5194/bg-2022-230
Preprint. Discussion started: 9 December 2022

conditions, estimation of T_{leaf} 2 °C lower than or equal to T_{air} may lead to significant bias in modeled leaf water isotope composition. Figure A3 shows that T_{plot} can be used to estimate T_{leaf}. The measurement of T_{plot} using IR radiometry as performed here is easy to set up and is strongly recommended if high accuracy is sought in the estimate of T_{leaf} at plot scale.

The $\delta^{18}O$ of atmospheric water vapor is often assumed to be in equilibrium with precipitation (e.g., Cernusak et al., 2002; Voelker et al., 2014; Bush et al., 2017; Li et al., 2017; Song et al., 2011; Flanagan and Farquhar, 2014). However, a recent comparison between modelled vapor and precipitation isotope compositions obtained from different isotope-enabled global climate models suggests that precipitation is rarely in equilibrium with atmospheric water vapor (Fiorella et al., 2019). The deviation generally increases with increasing latitude. In continental areas, the $\delta^{18}O$ of near-surface atmospheric water vapor can be lower than suggested by isotope equilibrium with precipitation due to high evaporation fluxes from lakes (Krabbenhoft et al., 1990; Benson and White, 1994). Similarly, the $\delta^{18}O$ of atmospheric water vapor can be lower than suggested by isotope equilibrium, if precipitation is affected by sub-cloud re-evaporation, as has been reported for monsoon areas (Landais et al., 2010; Wen et al., 2010). Moreover, the equilibrium assumption is often not valid in semi-arid to arid regions, when precipitation is limited to a short period of the year and not representative for the annual average atmospheric conditions (Tsujimura et al., 2007; Voigt et al., 2021). The atmospheric water vapor record presented here supports the validity of the equilibrium assumption at the study site, for annual $\delta^{18}O$, $\delta^{2}H$, d-excess and ^{17}O-excess averages. The agreement remains good at the monthly scale, but significant discrepancies occur for d-excess and ^{17}O-excess during the summer months when RH is the lowest. Sub-cloud re-evaporation of precipitation can be invoked to explain the low d-excess and ^{17}O-excess in precipitation whereas d-excess and ^{17}O-excess in the atmospheric water vapor stays stable. At the diurnal scale, primary isotope ratios of atmospheric water vapor can vary strongly, often deviating from the monthly equilibrium value. This can lead to significant model-data discrepancies (Fig. 4). ^{17}O-excess and d-excess of atmospheric water vapor generally agree with the monthly equilibrium water vapor at daytime, when transpiration is high, but significantly deviate at night and in the early morning. The use of the laser spectrometry should allow, in the near future, acquiring new records of the evolution of the isotope composition of atmospheric water vapor in different eco-climatic contexts to better understand the underlying processes at the different time scales. This will ultimately allow assessing whether the equilibrium assumption can be *a priori* applied to a given studied site.

4.3 The ^{17}O-excess of phytoliths reflects daily or daytime RH?

The relationship between $^{17}O\text{-excess}_{phyto}$ and RH was previously investigated in two growth chamber experiments where RH ranged from 40–80 % and T_{air} ranged from 20–28 °C. Differences in $\delta^{18}O$ values between source water and atmospheric water vapor were set to 0 ‰ in the first experiment (Alexandre et al., 2018) and to 10 ‰ in the second experiment (Outrequin et al., 2021). The two equations obtained from these experiments were statistically similar (Outrequin et al., 2021), and can be combined as follows:

https://doi.org/10.5194/bg-2022-230
Preprint. Discussion started: 9 December 2022


Biogeosciences Discussions Open Access EGU

$$RH = 0.22\ (\pm\ 0.01)\ {}^{17}O\text{-}excess_{phyto} + 115.2\ (\pm\ 3.9) \qquad (r^2 = 0.94) \qquad (6)$$

From the same datasets, a relationship between $^{17}O\text{-}excess_{phyto}$ and h can be obtained, assuming that T_{leaf} was 2 °C lower than T_{air}:

$$h = 0.25\ (\pm\ 0.02)\ {}^{17}O\text{-}excess_{phyto} + 130.0\ (\pm\ 4.4) \qquad (r^2 = 0.94) \qquad (7)$$

RH and h values reconstructed from $^{17}O\text{-}excess_{phyto}$ obtained for the three regrowths applying the above Eqs. (6) and (7) are closer to daytime averages (underestimation of RH by 4 ± 4 % and overestimation of h by 1 ± 5 %) than to daily averages (underestimation of RH by 12 ± 5 % and h by 6 ± 4 %) (Fig. 7, Table 2). While silica polymerization is metabolically controlled at the beginning of the leaf development, when the leaf emerges, silicification occurs mostly passively due to cell water saturation relative to silica during transpiration (Motomura et al., 2004; Kumar et al., 2017). In the present study, low stomatal conductance and transpiration measured on *F. arundinacea* likely hamper the phytolith formation at night, explaining that daytime RH determines $^{17}O\text{-}excess_{phyto}$. However, night-time stomatal conductance can vary across biomes, depending among others on plant functional types and soil moisture (Tobin and Kulmatiski, 2018; Resco de Dios et al., 2019). A recent data compilation reported that tropical trees show the highest stomatal conductance at night, followed by desert species (Resco de Dios et al., 2019). The lowest stomatal conductance was found for non-tropical evergreen angiosperms including Mediterranean species. Therefore, for a given case, the magnitude of night-time transpiration must be assessed to determine whether the RH reconstructed from $^{17}O\text{-}excess_{phyto}$ reflects day and night or only daytime conditions.

As expected from Eq. (1), reconstructed and measured daytime values obtained for h are in better agreement than for RH. However, the difference is lower than the uncertainty on the reconstructed values (4 %). A small amplitude of $T_{leaf\text{-}air}$, as observed in the present study (< 1.1 °C), have thus little impact on the RH estimates from $^{17}O\text{-}excess_{phyto}$. However, the possibility of larger amplitude, especially in the case of cold forests or warm desert areas should be considered to know if $^{17}O\text{-}excess_{phyto}$ is rather an indicator of RH or h.

https://doi.org/10.5194/bg-2022-230
Preprint. Discussion started: 9 December 2022

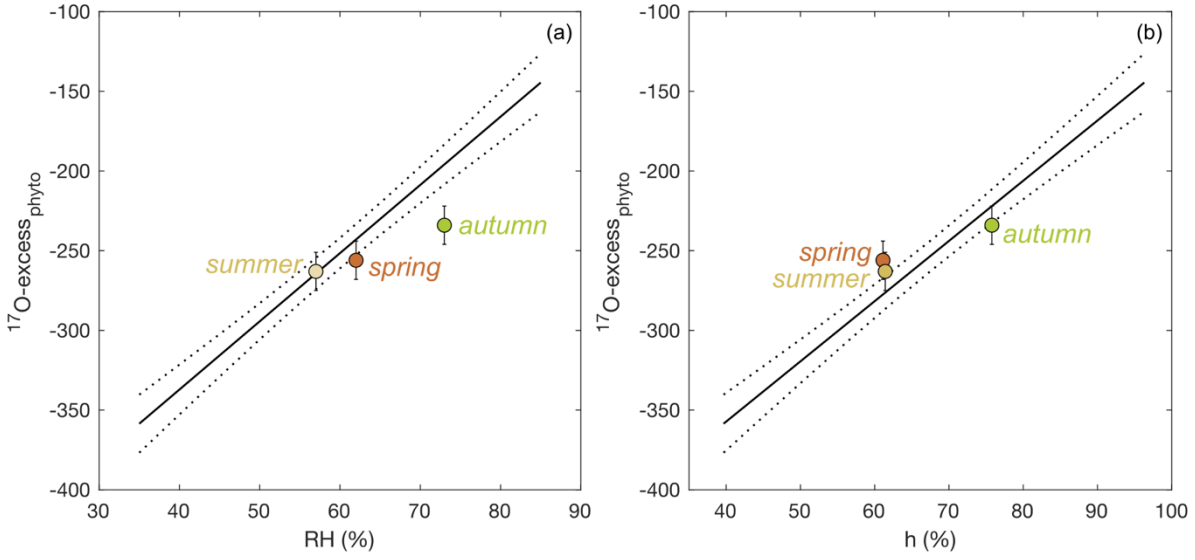

Figure 7: Observed ^{17}O-excess$_{phyto}$ vs average daytime (a) relative humidity (RH), and (b) water vapor pressure ratio between the leaf and the atmosphere (h), for regrowth periods in the spring, summer and autumn. The growth chamber calibration lines with 95 % confidence interval (Eqs. (6), (7)) are shown for comparison.

5 Conclusion

In this study, a model-data approach was used to interpret the diurnal and seasonal evolution of the triple oxygen isotope composition of *F. arundinacea* leaf water. All parameters relevant for modelling the triple oxygen isotope composition of grass leaf water were measured, including plot-scale grass leaf temperature and the triple oxygen isotope composition of atmospheric water vapor – two parameters that are often estimated as difficult to measure with accuracy. The results show that the steady state C-G model associated with a two-pool mixing equation reliably predicts the triple oxygen isotope composition of grass leaf water during daytime. The few model-data discrepancies (up to 4 ‰, 9 ‰, 34 per meg for δ^{18}O, d-excess and ^{17}O-excess, respectively) are related to differences between T_{plot} and actual T_{leaf}, variations in the fraction of the unevaporated water pool with changes in transpiration, and/or slight differences between measured RH close to the grass plot and actual RH right around the grass leaves. Deviations of the isotope composition of leaf water from steady state at night are well captured by the non-steady state model. We show that these deviations from steady-state can also be identified in the ^{17}O-excess vs δ'^{18}O system, whereas this is not the case in the d-excess vs δ^{18}O system. Measurements of the triple oxygen isotope composition of leaf water therefore can help to better constrain water transport processes from the plant to the atmosphere.

The difference between T_{leaf} and T_{air} is a key determinant on the isotope composition of leaf water. Under the study conditions, it is close to -2 °C at midday, which is in line with the temperature measurements previously performed on *F. arundinacea* in climate-controlled growth chambers (Alexandre et al., 2019). To gain further insights into this parameter and its variability

https://doi.org/10.5194/bg-2022-230
Preprint. Discussion started: 9 December 2022

according to vegetation and climate types, we recommend IR radiometer measurements with spatial coverage as carried out in the present study.

The first continuous record of atmospheric water vapor including $\delta^{17}O$ measurement presented here shows that although $\delta^{17}O$, $\delta^{18}O$ and $\delta^{2}H$ are highly variable at the daily scale, assuming equilibrium between precipitation and atmospheric water vapor isotope composition is reasonable for these first order parameters at the monthly and annual scales. The second order parameters d-excess and ^{17}O-excess vary little at the daily, monthly and annual scales and are always close to the equilibrium values estimated from precipitation. Further records of the triple oxygen isotope composition of the atmospheric water vapor, facilitated by the use of laser spectrometers, and precipitation will help to generalize this result.

Further, we examined how leaf-to-air temperature gradients and changes in the silica polymerization rate in response to stomatal conductance influence the interpretation of $^{17}O\text{-excess}_{phyto}$ in terms of RH. The measured values of $^{17}O\text{-excess}_{phyto}$ and daytime RH fit well with the $^{17}O\text{-excess}_{phyto}$ vs RH equation established from previous growth chamber experiments (Alexandre et al., 2018; Outrequin et al., 2021). Relationships between $^{17}O\text{-excess}_{phyto}$, stomatal conductance and RH observed in this study suggest that the magnitude of night-time stomatal conductance and transpiration needs to be assessed in each study individually to evaluate if RH reconstructed from $^{17}O\text{-excess}_{phyto}$ reflects daily or daytime conditions. Small leaf-to-air temperature gradients of less than 2 °C as observed in the present study have little impact on the RH estimates from $^{17}O\text{-excess}_{phyto}$. However, large difference between T_{leaf} and T_{air} as common in cold forests or warm desert vegetation should be considered when reconstructing RH using $^{17}O\text{-excess}_{phyto}$ in these contexts. The insights gained from this study allow to better understand the RH proxy that is $^{17}O\text{-excess}_{phyto}$. The study also confirms the consistency of $^{18}\alpha_{phyto\text{-}H2O}$ and $\lambda_{phyto\text{-}H2O}$, which opens perspectives for reconstructing past changes in leaf water isotope composition from the triple oxygen isotope composition of fossil phytoliths recovered from buried soils and sediments, e.g., useful for land-surface model and data comparisons.

https://doi.org/10.5194/bg-2022-230
Preprint. Discussion started: 9 December 2022

Biogeosciences Discussions Open Access EGU

Appendices

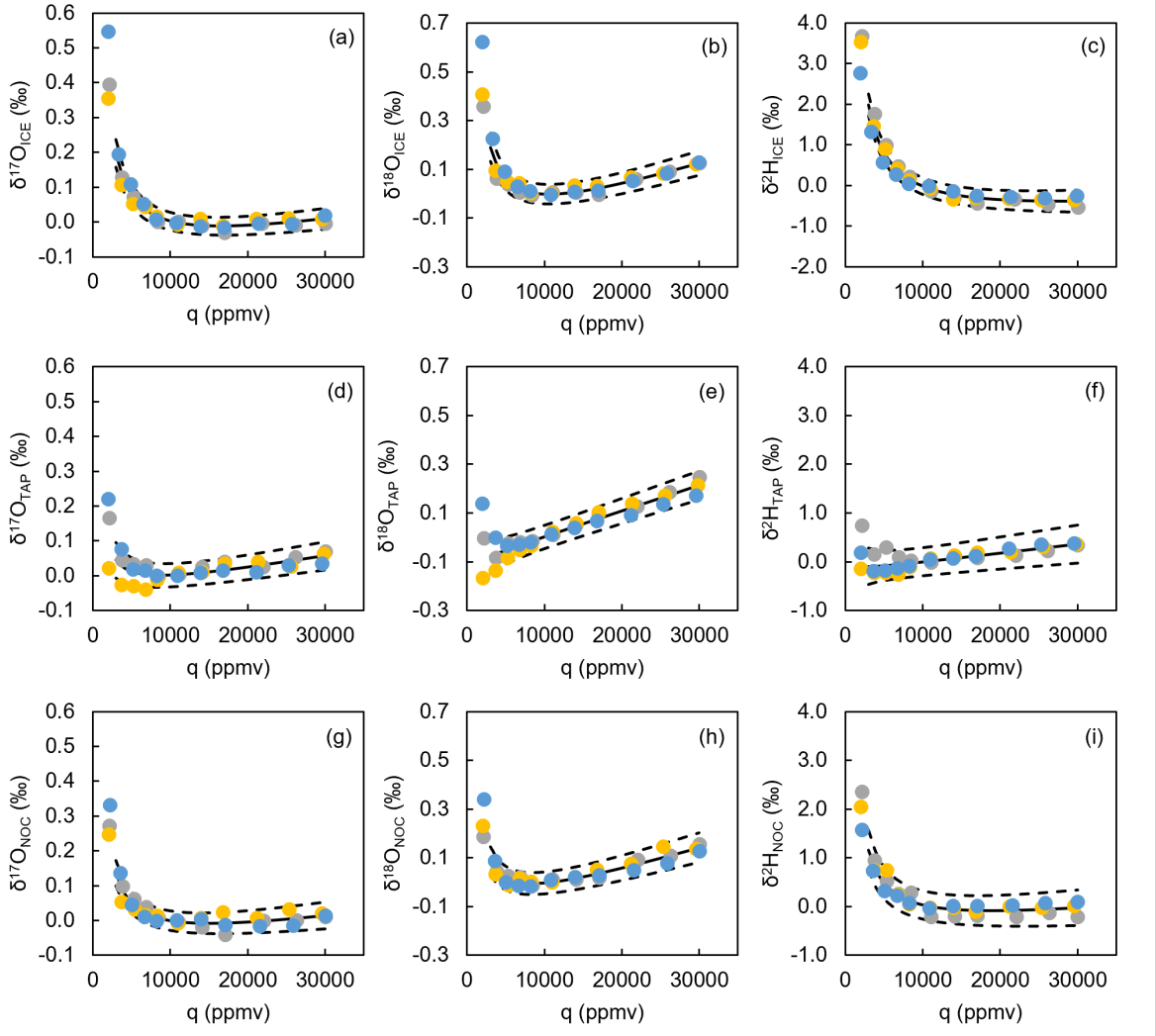

Figure A1: Water mixing ratio dependencies of $\delta^{17}O$, $\delta^{18}O$ and $\delta^{2}H$ normalized to the isotope composition measured at a water mixing ratio (q) of 10000 ppmv for the three water standards ((a)–(c) ICE ($\delta^{18}O$ = -26.85‰), (d)–(f) NOC ($\delta^{18}O$ = -16.91‰), (g)–(i) TAP ($\delta^{18}O$ = -8.64‰)). Mixing ratio dependency calibrations were performed on 26 May 2021 (grey), 20 October 2021 (yellow), and 05 January 2022 (blue). Solid and dashed lines show mean and 1 standard deviation of the mixing ratio dependency function.

https://doi.org/10.5194/bg-2022-230
Preprint. Discussion started: 9 December 2022

Biogeosciences
Discussions
Open Access
EGU

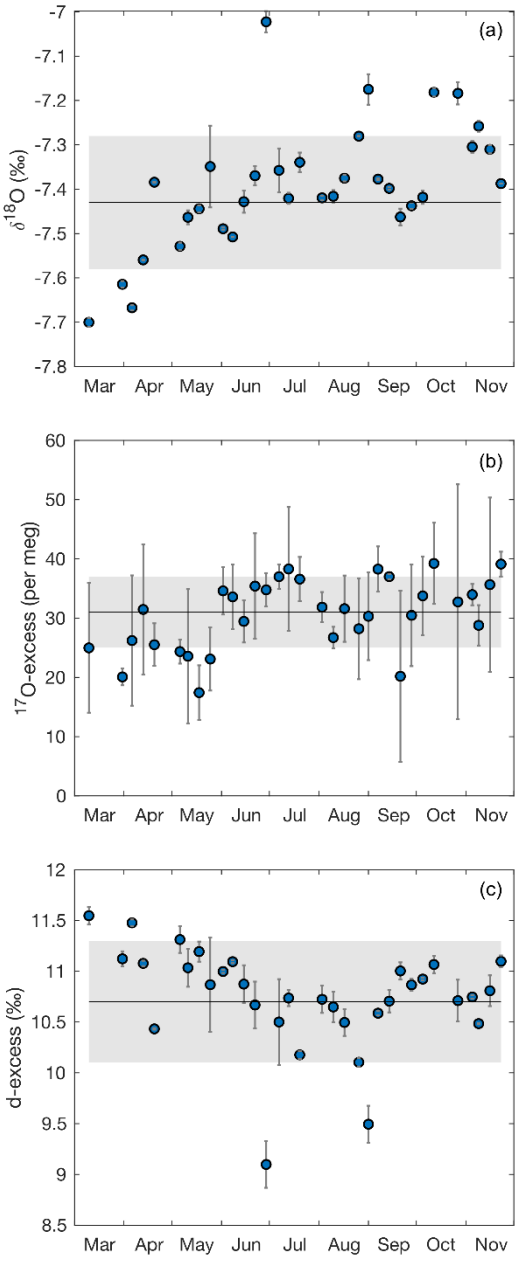

Fig A2: Evolution of (a) $\delta^{18}O$, (b) ^{17}O-excess and (c) d-excess of the irrigation water from March to November 2021. Each data point represents the average isotope composition of the irrigation water over the period between two samples. Error bars are 1 standard deviation (SD). The solid lines and the grey shaded areas indicate mean and SD of the isotope composition of irrigation water averaged over all samples.

https://doi.org/10.5194/bg-2022-230
Preprint. Discussion started: 9 December 2022

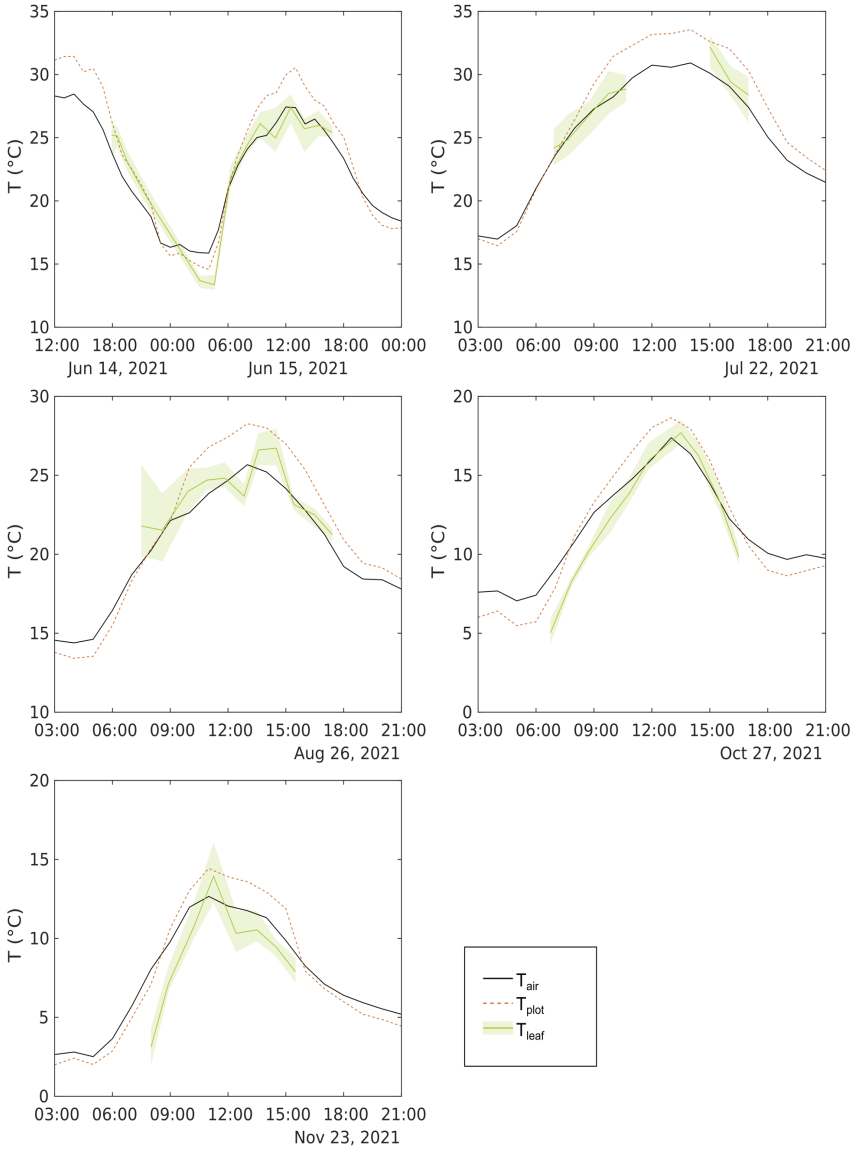

Figure A3: Diurnal evolution of atmospheric temperature (T_{air}), plot-scale grass leaf temperature (T_{plot}) and mean and 1 standard deviation of leaf temperature measurements on single leaves using the optris IR thermometer (T_{leaf}) measured on field days between April and November 2021.

https://doi.org/10.5194/bg-2022-230
Preprint. Discussion started: 9 December 2022

600

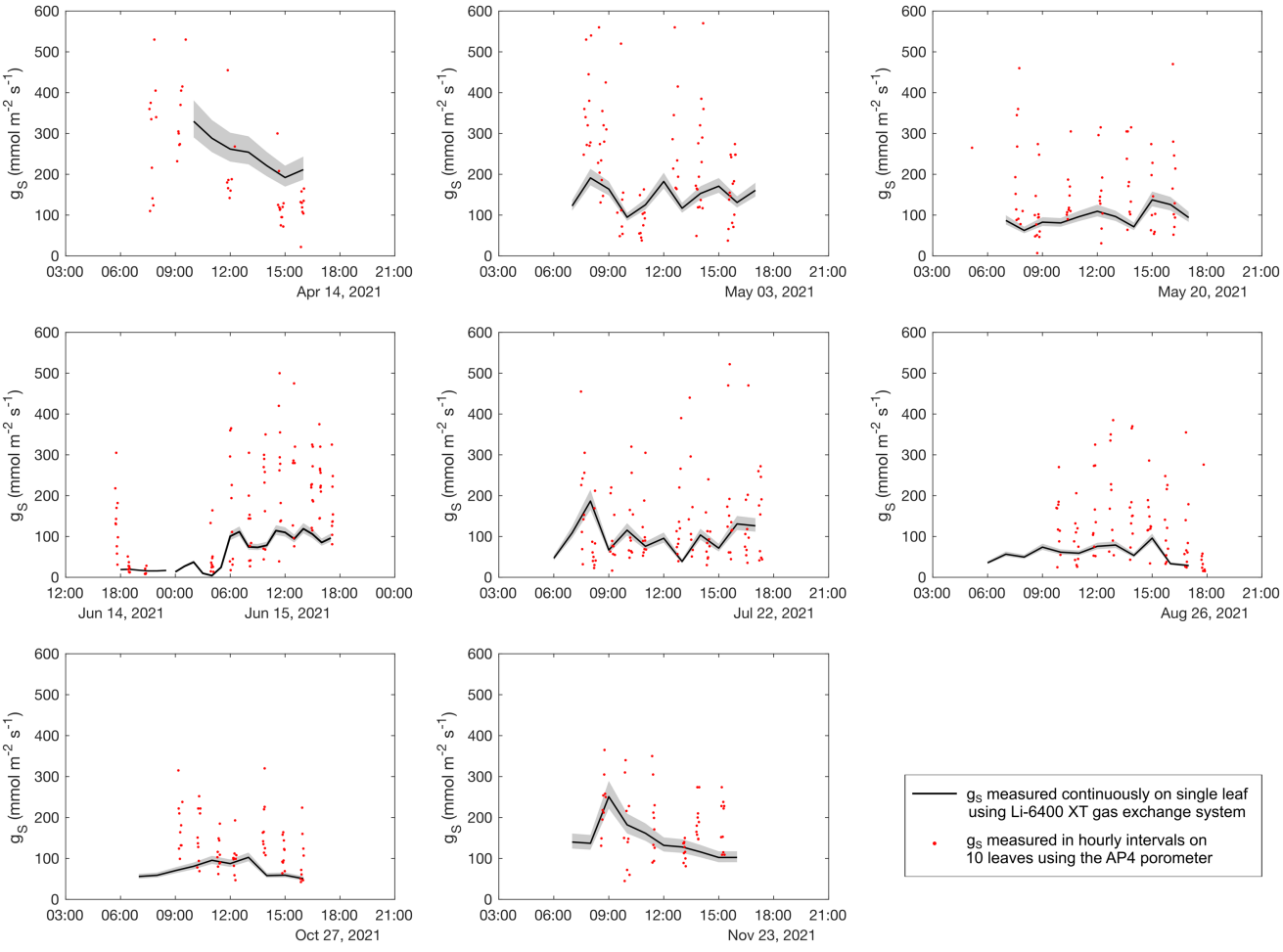

Figure A4: Diurnal evolution of stomatal conductance (g_s) measured on field days between April and November 2021. Black lines show g_s of a single grass leaf measured continuously over the day using the Li-COR gas exchange system in hourly resolution. Red points represent g_s of different grass leaves measured with the AP4 porometer.

https://doi.org/10.5194/bg-2022-230
Preprint. Discussion started: 9 December 2022

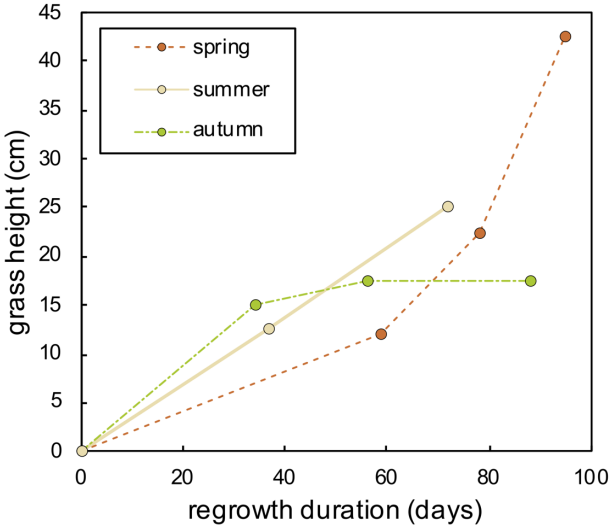

Figure A5: Evolution of the grass height over the regrowth duration from 17 February–20 May 2021 (spring), from 15 June–27 August 2021 (summer) and from 27 August–23 November 2021 (autumn).

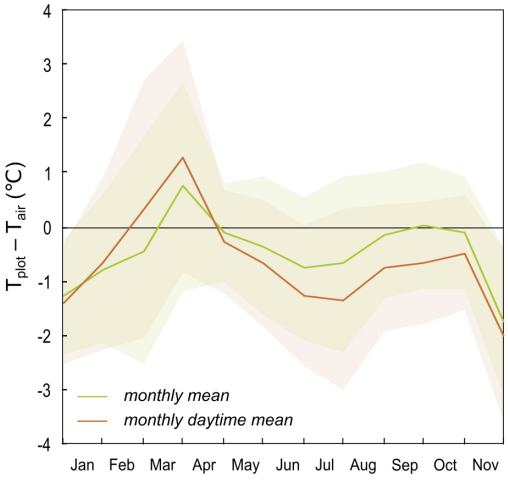

Figure A6: Monthly mean and daytime mean of the difference between plot-scale grass leaf temperature (T_{plot}) and air temperature (T_{air}). The shaded area represents 1 standard deviation.

Data availability

Data available within the article or its supplementary materials. Additional data will be made available on request. Climate data can be accessed from the COOPERATE database: https://cooperate.eccorev.fr/db.

https://doi.org/10.5194/bg-2022-230
Preprint. Discussion started: 9 December 2022

Author contribution

AA conceptualized the project and acquired financial support. AA, CV, CVC, IR, JPO and CP designed the experiments and carried out field work. CV, AA, JCM, CVC, and HM performed laboratory analyses. CV and AA prepared the manuscript with contributions from all co-authors.

Competing interests

The authors declare that they have no conflict of interest.

Acknowledgements

We acknowledge Martine Couapel for her help with the field experiments. We thank Nicholas Devert and Sabrina Dubois for performing leaf water extractions at ISPA, Bordeaux. We thank the team of the Stable Isotope Laboratory at the University of Cologne under the leadership of Michael Staubwasser for permission of and support during leaf water triple oxygen and hydrogen isotope analyses in their laboratory. Our research was conducted in the frame of the HUMI-17 project supported by the ANR (grant nos. ANR-17-CE01-0002-01), CNRS FR3098 ECCOREV, LABEX OT-Med and OSU-Pytheas. It benefited from the CNRS human and technical resources allocated to the Ecotron Research Infrastructure from the state allocation "Investissement d'Avenir" AnaEE France ANR-11-INBS-0001.

References

Alexandre, A., Basile-Doelsch, I., Sonzogni, C., Sylvestre, F., Parron, C., Meunier, J. D., and Colin, F.: Oxygen isotope analyses of fine silica grains using laser-extraction technique: Comparison with oxygen isotope data obtained from ion microprobe analyses and application to quartzite and silcrete cement investigation, Geochim. Cosmochim. Acta, 70, 2827–2835, https://doi.org/10.1016/j.gca.2006.03.003, 2006.

Alexandre, A., Landais, A., Vallet-Coulomb, C., Piel, C., Devidal, S., Pauchet, S., Sonzogni, C., Couapel, M., Pasturel, M., Cornuault, P., Xin, J., Mazur, J. C., Prié, F., Bentaleb, I., Webb, E., Chalié, F., and Roy, J.: The triple oxygen isotope composition of phytoliths as a proxy of continental atmospheric humidity: Insights from climate chamber and climate transect calibrations, Biogeosciences, 15, 3223–3241, https://doi.org/10.5194/bg-15-3223-2018, 2018.

Alexandre, A., Webb, E., Landais, A., Piel, C., Devidal, S., Sonzogni, C., Couapel, M., Mazur, J., Pierre, M., Prié, F., Vallet-Coulomb, C., Outrequin, C., and Roy, J.: Effects of leaf length and development stage on the triple oxygen isotope signature of grass leaf water and phytoliths: insights for a proxy of continental atmospheric humidity, Biogeosciences, 16, 4613–4625, https://doi.org/10.5194/bg-16-4613-2019, 2019.

Apogee Instruments Inc: https://www.apogeeinstruments.com/blog/emissivity-correction/, last access: 8 June 2022.

Aron, P. G., Levin, N. E., Beverly, E. J., Huth, T. E., Passey, B. H., Pelletier, E. M., Poulsen, C. J., Winkelstern, I. Z., and Yarian, D. A.: Triple oxygen isotopes in the water cycle, Chem. Geol., 565, 120026, https://doi.org/10.1016/j.chemgeo.2020.120026, 2021.

Barbeta, A., Burlett, R., Martín-Gómez, P., Fréjaville, B., Devert, N., Wingate, L., Domec, J. C., and Ogée, J.: Evidence for distinct isotopic compositions of sap and tissue water in tree stems: consequences for plant water source identification, New Phytol., 233, 1121–1132,

https://doi.org/10.1111/nph.17857, 2022.

Barbour, M. M., Loucos, K. E., Lockhart, E. L., Shrestha, A., McCallum, D., Simonin, K. A., Song, X., Griffani, D. S., and Farquhar, G. D.: Can hydraulic design explain patterns of leaf water isotopic enrichment in C_3 plants?, Plant. Cell Environ., 44, 432–444, https://doi.org/10.1111/pce.13943, 2021.

Barkan, E. and Luz, B.: High precision measurements of $^{17}O/^{16}O$ and $^{18}O/^{16}O$ ratios in H_2O, Rapid Commun. Mass Spectrom., 19, 3737–3742, https://doi.org/10.1002/rcm.2250, 2005.

Barkan, E. and Luz, B.: Diffusivity fractionations of $H_2{}^{16}O/H_2{}^{17}O$ and $H_2{}^{16}O/H_2{}^{18}O$ in air and their implications for isotope hydrology, Rapid Commun. Mass Spectrom., 21, 2999–3005, https://doi.org/10.1002/rcm.3180, 2007.

Belviso, S., Marco Reiter, I., Loubet, B., Gros, V., Lathière, J., Montagne, D., Delmotte, M., Ramonet, M., Kalogridis, C., Lebegue, B., Bonnaire, N., Kazan, V., Gauquelin, T., Fernandez, C., and Genty, B.: A top-down approach of surface carbonyl sulfide exchange by a Mediterranean oak forest ecosystem in southern France, Atmos. Chem. Phys., 16, 14909–14923, https://doi.org/10.5194/acp-16-14909-2016, 2016.

Benson, L. V. and White, J. W. C.: Stable isotopes of oxygen and hydrogen in the Truckee River-Pyramid Lake surface-water system. 3. Source of water vapor overlying Pyramid Lake, Limnol. Oceanogr., 39, 1945–1958, https://doi.org/10.4319/lo.1994.39.8.1945, 1994.

Blonder, B. and Michaletz, S. T.: A model for leaf temperature decoupling from air temperature, Agric. For. Meteorol., 262, 354–360, https://doi.org/10.1016/j.agrformet.2018.07.012, 2018.

Bögelein, R., Thomas, F. M., and Kahmen, A.: Leaf water ^{18}O and ^{2}H enrichment along vertical canopy profiles in a broadleaved and a conifer forest tree, Plant Cell Environ., 40, 1086–1103, https://doi.org/10.1111/pce.12895, 2017.

Bush, R. T., Berke, M. A., and Jacobson, A. D.: Plant Water δD and $\delta^{18}O$ of Tundra Species from West Greenland, Arctic, Antarct. Alp. Res., 49, 341–358, https://doi.org/10.1657/AAAR0016-025, 2017.

Cernusak, L. A., Pate, J. S., and Farquhar, G. D.: Diurnal variation in the stable isotope composition of water and dry matter in fruiting Lupinus angustifolius under field conditions, Plant, Cell Environ., 25, 893–907, https://doi.org/10.1046/j.1365-3040.2002.00875.x, 2002.

Cernusak, L. A., Barbour, M. M., Arndt, S. K., Cheesman, A. W., English, N. B., Feild, T. S., Helliker, B. R., Holloway-Phillips, M. M., Holtum, J. A. M., Kahmen, A., Mcinerney, F. A., Munksgaard, N. C., Simonin, K. A., Song, X., Stuart-Williams, H., West, J. B., and Farquhar, G. D.: Stable isotopes in leaf water of terrestrial plants, Plant Cell Environ., 39, 1087–1102, https://doi.org/10.1111/pce.12703, 2016.

Chapligin, B., Meyer, H., Friedrichsen, H., Marent, A., Sohns, E., and Hubberten, H.-W.: A high-performance, safer and semi-automated approach for the $\delta^{18}O$ analysis of diatom silica and new methods for removing exchangeable oxygen, Rapid Commun. Mass Spectrom., 24, 2655–2664, https://doi.org/10.1002/rcm.4689, 2010.

Corbineau, R., Reyerson, P. E., Alexandre, A., and Santos, G. M.: Towards producing pure phytolith concentrates from plants that are suitable for carbon isotopic analysis, Rev. Palaeobot. Palynol., 197, 179–185, https://doi.org/10.1016/j.revpalbo.2013.06.001, 2013.

Craig, H. and Gordon, L. I.: Deuterium and oxygen 18 variations in the ocean and the marine atmosphere, in: Stable Isotopes in Oceanographic Studies and Paleotemperatures, 9–130, 1965.

Crespin, J., Alexandre, A., Sylvestre, F., Sonzogni, C., Paillès, C., and Garreta, V.: IR laser extraction technique applied to oxygen isotope analysis of small biogenic silica samples, Anal. Chem., 80, 2372–2378, https://doi.org/10.1021/ac071475c, 2008.

Cuntz, M., Ogée, J., Farquhar, G. D., Peylin, P., and Cernusak, L. A.: Modelling advection and diffusion of water isotopologues in leaves, Plant, Cell Environ., 30, 892–909, https://doi.org/10.1111/j.1365-3040.2007.01676.x, 2007.

Dodd, J. P. and Sharp, Z. D.: A laser fluorination method for oxygen isotope analysis of biogenic silica and a new oxygen isotope calibration of modern diatoms in freshwater environments, Geochim. Cosmochim. Acta, 74, 1381–1390, https://doi.org/10.1016/j.gca.2009.11.023, 2010.

https://doi.org/10.5194/bg-2022-230
Preprint. Discussion started: 9 December 2022

Dongmann, G., Nürnberg, H. W., Förstel, H., and Wagener, K.: On the enrichment of $H_2{}^{18}O$ in the leaves of transpiring plants, Radiat. Environ. Biophys., 11, 41–52, https://doi.org/10.1007/BF01323099, 1974.

Farquhar, G. D. and Cernusak, L. A.: On the isotopic composition of leaf water in the non-steady state, Funct. Plant Biol., 32, 293–303, https://doi.org/10.1071/FP04232, 2005.

Farquhar, G. D. and Lloyd, J.: Carbon and Oxygen Isotope Effects in the Exchange of Carbon Dioxide between Terrestrial Plants and the Atmosphere, in: Stable Isotopes and Plant Carbon-Water Relations, Academic Press, 47–70, https://doi.org/10.1016/B978-0-08-091801-3.50011-8, 1993.

Farquhar, G. D., Cernusak, L. A., and Barnes, B.: Heavy Water Fractionation during Transpiration, Plant Physiol., 143, 11–18, https://doi.org/10.1104/pp.106.093278, 2007.

Farris, F. and Strain, B. R.: The effects of water-stress on leaf $H_2{}^{18}O$ enrichment, Radiat. Environ. Biophys., 15, 167–202, https://doi.org/10.1007/BF01323264, 1978.

Fiorella, R. P., West, J. B., and Bowen, G. J.: Biased estimates of the isotope ratios of steady-state evaporation from the assumption of equilibrium between vapour and precipitation, Hydrol. Process., 33, 2576–2590, https://doi.org/10.1002/hyp.13531, 2019.

Flanagan, L. B. and Farquhar, G. D.: Variation in the carbon and oxygen isotope composition of plant biomass and its relationship to water-use efficiency at the leaf- and ecosystem-scales in a northern Great Plains grassland, Plant, Cell Environ., 37, 425–438, https://doi.org/10.1111/pce.12165, 2014.

Flanagan, L. B., Comstock, J. P., and Ehleringer, J. R.: Comparison of Modeled and Observed Environmental Influences on the Stable Oxygen and Hydrogen Isotope Composition of Leaf Water in Phaseolus vulgaris L., Plant Physiol., 96, 588–596, https://doi.org/10.1104/pp.96.2.588, 1991.

Gan, K. S., Wong, S. C., Yong, J. W. H., and Farquhar, G. D.: ^{18}O Spatial Patterns of Vein Xylem Water, Leaf Water, and Dry Matter in Cotton Leaves, Plant Physiol., 130, 1008–1021, https://doi.org/10.1104/pp.007419, 2002.

Garcin, Y., Schwab, V. F., Gleixner, G., Kahmen, A., Todou, G., Séné, O., Onana, J. M., Achoundong, G., and Sachse, D.: Hydrogen isotope ratios of lacustrine sedimentary n-alkanes as proxies of tropical African hydrology: Insights from a calibration transect across Cameroon, Geochim. Cosmochim. Acta, 79, 106–126, https://doi.org/10.1016/j.gca.2011.11.039, 2012.

Gröning, M., Lutz, H. O., Roller-Lutz, Z., Kralik, M., Gourcy, L., and Pöltenstein, L.: A simple rain collector preventing water re-evaporation dedicated for $\delta^{18}O$ and $\delta^{2}H$ analysis of cumulative precipitation samples, J. Hydrol., 448–449, 195–200, https://doi.org/10.1016/j.jhydrol.2012.04.041, 2012.

Grossiord, C., Buckley, T. N., Cernusak, L. A., Novick, K. A., Poulter, B., Siegwolf, R. T. W., Sperry, J. S., and McDowell, N. G.: Plant responses to rising vapor pressure deficit, New Phytol., 226, 1550–1566, https://doi.org/10.1111/nph.16485, 2020.

Helliker, B. R. and Ehleringer, J. R.: Differential 18O enrichment of leaf cellulose in C3 versus C4 grasses, Funct. Plant Biol., 29, 435–442, https://doi.org/10.1071/PP01122, 2002a.

Helliker, B. R. and Ehleringer, J. R.: Grass blades as tree rings: Environmentally induced changes in the oxygen isotope ratio of cellulose along the length of grass blades, New Phytol., 155, 417–424, https://doi.org/10.1046/j.1469-8137.2002.00480.x, 2002b.

Hirl, R. T., Schnyder, H., Ostler, U., Schäufele, R., Schleip, I., Vetter, S. H., Auerswald, K., Baca Cabrera, J. C., Wingate, L., Barbour, M. M., and Ogée, J.: The ^{18}O ecohydrology of a grassland ecosystem - predictions and observations, Hydrol. Earth Syst. Sci., 23, 2581–2600, https://doi.org/10.5194/hess-23-2581-2019, 2019.

Holloway-Phillips, M., Cernusak, L. A., Barbour, M., Song, X., Cheesman, A., Munksgaard, N., Stuart-Williams, H., and Farquhar, G. D.: Leaf vein fraction influences the Péclet effect and ^{18}O enrichment in leaf water, Plant Cell Environ., 39, 2414–2427, https://doi.org/10.1111/pce.12792, 2016.

IPCC: Climate Change 2013: The Physical Science Basis. Contribution of Working Group I to the Fifth Assessment Report of the

Intergovernmental Panel on Climate Change, edited by: Stocker, T. F., Qin, D., Plattner, G.-K., Tignor, M., Allen, S. K., Boschung, J., Nauels, A., Xia, Y., Bex, V., and Midgley, P. M., Cambridge University Press, Cambridge, United Kingdom and New York, NY, US, 1585 pp. pp., 2013.

IUSS Working Group WRB: World Reference Base for Soil Resources 2014, update 2015. International soil classification system for naming soils and creating legends for soil maps, World Soil Resources Reports No. 106, FAO, Rome, 2015.

Kahmen, A., Sachse, D., Arndt, S. K., Tu, K. P., Farrington, H., Vitousek, P. M., and Dawsona, T. E.: Cellulose $\delta^{18}O$ is an index of leaf-to-air vapor pressure difference (VPD) in tropical plants, Proc. Natl. Acad. Sci. U. S. A., 108, 1981–1986, https://doi.org/10.1073/pnas.1018906108, 2011.

Kahmen, A., Schefuß, E., and Sachse, D.: Leaf water deuterium enrichment shapes leaf wax n-alkane δD values of angiosperm plants I: Experimental evidence and mechanistic insights, Geochim. Cosmochim. Acta, 111, 39–49, https://doi.org/10.1016/j.gca.2012.09.003, 2013.

Krabbenhoft, D. P., Bowser, C. J., Anderson, M. P., and Valley, J. W.: Estimating groundwater exchange with lakes: 1. The stable isotope mass balance method, Water Resour. Res., 26, 2445–2453, https://doi.org/10.1029/WR026i010p02445, 1990.

Kumar, S., Soukup, M., and Elbaum, R.: Silicification in grasses: Variation between different cell types, Front. Plant Sci., 8, 1–8, https://doi.org/10.3389/fpls.2017.00438, 2017.

Landais, A., Risi, C., Bony, S., Vimeux, F., Descroix, L., Falourd, S., and Bouygues, A.: Combined measurements of $^{17}O_{excess}$ and d-excess in African monsoon precipitation: Implications for evaluating convective parameterizations, Earth Planet. Sci. Lett., 298, 104–112, https://doi.org/10.1016/j.epsl.2010.07.033, 2010.

Leaney, F. W., Osmond, C. B., Allison, G. B., and Ziegler, H.: Hydrogen-isotope composition of leaf water in C_3 and C_4 plants: its relationship to the hydrogen-isotope composition of dry matter, Planta, 164, 215–220, https://doi.org/10.1007/BF00396084, 1985.

Leuzinger, S. and Körner, C.: Tree species diversity affects canopy leaf temperatures in a mature temperate forest, Agric. For. Meteorol., 146, 29–37, https://doi.org/10.1016/j.agrformet.2007.05.007, 2007.

Li, S., Levin, N. E., Soderberg, K., Dennis, K. J., and Caylor, K. K.: Triple oxygen isotope composition of leaf waters in Mpala, central Kenya, Earth Planet. Sci. Lett., 468, 38–50, https://doi.org/10.1016/j.epsl.2017.02.015, 2017.

Liu, P., Liu, J., Ji, A., Reinhard, C. T., Planavsky, N. J., Babikov, D., Najjar, R. G., and Kasting, J. F.: Triple oxygen isotope constraints on atmospheric O_2 and biological productivity during the mid-Proterozoic, Proc. Natl. Acad. Sci. U. S. A., 118, https://doi.org/10.1073/pnas.2105074118, 2021.

López, J., Way, D. A., and Sadok, W.: Systemic effects of rising atmospheric vapor pressure deficit on plant physiology and productivity, Glob. Chang. Biol., 27, 1704–1720, https://doi.org/10.1111/gcb.15548, 2021.

Loucos, K. E., Simonin, K. A., Song, X., and Barbour, M. M.: Observed relationships between leaf $H_2{}^{18}O$ Péclet effective length and leaf hydraulic conductance reflect assumptions in Craig-Gordon model calculations, Tree Physiol., 35, 16–26, https://doi.org/10.1093/treephys/tpu110, 2014.

Luz, B. and Barkan, E.: Variations of $^{17}O/^{16}O$ and $^{18}O/^{16}O$ in meteoric waters, Geochim. Cosmochim. Acta, 74, 6276–6286, https://doi.org/10.1016/j.gca.2010.08.016, 2010.

Merlivat, L.: Molecular diffusivities of $H_2{}^{16}O$, $HD^{16}O$, and $H_2{}^{18}O$ in gases, J. Chem. Phys., 69, https://doi.org/https://doi.org/10.1063/1.436884, 1978.

Monteith, J.: Evaporation and environment, Symp. Soc. Exp. Biol., 19, 205–234, 1965.

Motomura, H., Fujii, T., and Suzuki, M.: Silica deposition in relation to ageing of leaf tissues in Sasa veitchii (Carrière) Rehder (Poaceae: Bambusoideae), Ann. Bot., 93, 235–248, https://doi.org/10.1093/aob/mch034, 2004.

Ogée, J., Cuntz, M., Peylin, P., and Bariac, T.: Non-steady-state, non-uniform transpiration rate and leaf anatomy effects on the progressive

765 stable isotope enrichment of leaf water along monocot leaves, Plant, Cell Environ., 30, 367–387, https://doi.org/10.1111/j.1365-3040.2006.01621.x, 2007.

Outrequin, C., Alexandre, A., Vallet-Coulomb, C., Piel, C., Devidal, S., Landais, A., Couapel, M., Mazur, J., Peugeot, C., Pierre, M., Prié, F., Roy, J., Sonzogni, C., and Voigt, C.: The triple oxygen isotope composition of phytoliths, a new proxy of atmospheric relative humidity: controls of soil water isotope composition, temperature, CO_2 concentration and relative humidity, Clim. Past Discuss., 17, 1881–1902, 770 https://doi.org/10.5194/cp-17-1881-2021, 2021.

COOPERATE database: https://cooperate.eccorev.fr/db, last access: 8 June 2022.

Resco de Dios, V., Chowdhury, F. I., Granda, E., Yao, Y., and Tissue, D. T.: Assessing the potential functions of nocturnal stomatal conductance in C_3 and C_4 plants, New Phytol., 223, 1696–1706, https://doi.org/10.1111/nph.15881, 2019.

Rey-Sánchez, A. C., Slot, M., Posada, J. M., and Kitajima, K.: Spatial and seasonal variation in leaf temperature within the canopy of a 775 tropical forest, Clim. Res., 71, 75–89, https://doi.org/10.3354/cr01427, 2016.

Royles, J., Ogée, J., Wingate, L., Hodgson, D. A., Convey, P., and Griffiths, H.: Temporal separation between CO_2 assimilation and growth? Experimental and theoretical evidence from the desiccation-tolerant moss Syntrichia ruralis, New Phytol., 197, 1152–1160, https://doi.org/10.1111/nph.12114, 2013.

Sharp, Z. D., Gibbons, J. A., Maltsev, O., Atudorei, V., Pack, A., Sengupta, S., Shock, E. L., and Knauth, L. P.: A calibration of the triple 780 oxygen isotope fractionation in the SiO_2-H_2O system and applications to natural samples, Geochim. Cosmochim. Acta, 186, 105–119, https://doi.org/10.1016/j.gca.2016.04.047, 2016.

Siebert, S., Ewert, F., Eyshi Rezaei, E., Kage, H., and Graß, R.: Impact of heat stress on crop yield - On the importance of considering canopy temperature, Environ. Res. Lett., 9, 044012, https://doi.org/10.1088/1748-9326/9/4/044012, 2014.

Song, X., Barbour, M. M., Saurer, M., and Helliker, B. R.: Examining the large-scale convergence of photosynthesis-weighted tree leaf 785 temperatures through stable oxygen isotope analysis of multiple data sets, New Phytol., 192, 912–924, https://doi.org/10.1111/j.1469-8137.2011.03851.x, 2011.

Song, X., Simonin, K. A., Loucos, K. E., and Barbour, M. M.: Modelling non-steady-state isotope enrichment of leaf water in a gas-exchange cuvette environment, Plant Cell Environ., 38, 2618–2628, https://doi.org/10.1111/pce.12571, 2015.

Still, C., Powell, R., Aubrecht, D., Kim, Y., Helliker, B., Roberts, D., Richardson, A. D., and Goulden, M.: Thermal imaging in plant and 790 ecosystem ecology: applications and challenges, Ecosphere, 10, https://doi.org/10.1002/ecs2.2768, 2019.

Surma, J., Assonov, S., Bolourchi, M. J., and Staubwasser, M.: Triple oxygen isotope signatures in evaporated water bodies from the Sistan Oasis, Iran, Geophys. Res. Lett., 42, 8456–8462, https://doi.org/10.1002/2015GL066475, 2015.

Surma, J., Assonov, S., and Staubwasser, M.: Triple Oxygen Isotope Systematics in the Hydrologic Cycle, Rev. Mineral. Geochemistry, 86, 401–428, https://doi.org/10.2138/rmg.2021.86.12, 2021.

795 Tierney, J. E., Poulsen, C. J., Montañez, I. P., Bhattacharya, T., Feng, R., Ford, H. L., Hönisch, B., Inglis, G. N., Petersen, S. V., Sagoo, N., Tabor, C. R., Thirumalai, K., Zhu, J., Burls, N. J., Foster, G. L., Goddéris, Y., Huber, B. T., Ivany, L. C., Turner, S. K., Lunt, D. J., McElwain, J. C., Mills, B. J. W., Otto-Bliesner, B. L., Ridgwell, A., and Zhang, Y. G.: Past climates inform our future, Science, 370, eaay3701, https://doi.org/10.1126/science.aay3701, 2020.

Tobin, R. L. and Kulmatiski, A.: Plant identity and shallow soil moisture are primary drivers of stomatal conductance in the savannas of 800 Kruger National Park, PLoS One, 13, 1–17, https://doi.org/10.1371/journal.pone.0191396, 2018.

Tsujimura, M., Sasaki, L., Yamanaka, T., Sugimoto, A., Li, S. G., Matsushima, D., Kotani, A., and Saandar, M.: Vertical distribution of stable isotopic composition in atmospheric water vapor and subsurface water in grassland and forest sites, eastern Mongolia, J. Hydrol., 333, 35–46, https://doi.org/10.1016/j.jhydrol.2006.07.025, 2007.

Tuthorn, M., Zech, R., Ruppenthal, M., Oelmann, Y., Kahmen, A., del Valle, H. F., Eglinton, T., Rozanski, K., and Zech, M.: Coupling δ^2H

805 and $\delta^{18}O$ biomarker results yields information on relative humidity and isotopic composition of precipitation – a climate transect validation study, Biogeosciences, 12, 3913–3924, https://doi.org/10.5194/bg-12-3913-2015, 2015.

Vallet-Coulomb, C., Couapel, M., and Sonzogni, C.: Improving memory effect correction to achieve high precision analysis of $\delta^{17}O$, $\delta^{18}O$ $\delta^{2}H$, ^{17}O-excess and d-excess in water using cavity ring-down laser spectroscopy, Rapid Commun. Mass Spectrom., 35, e9108, https://doi.org/10.1002/rcm.9108, 2021.

810 Voelker, S. L., Brooks, J. R., Meinzer, F. C., Roden, J., Pazdur, A., Pawelczyk, S., Hartsough, P., Snyder, K., Plavcová, L., and Šantruček, J.: Reconstructing relative humidity from plant δ18O and δD as deuterium deviations from the global meteoric water line, Ecol. Appl., 24, 960–975, https://doi.org/10.1890/13-0988.1, 2014.

Voigt, C., Herwartz, D., Dorador, C., and Staubwasser, M.: Triple oxygen isotope systematics of evaporation and mixing processes in a dynamic desert lake system, Hydrol. Earth Syst. Sci., 25, 1211–1228, https://doi.org/10.5194/hess-25-1211-2021, 2021.

815 Voigt, C., Vallet-Coulomb, C., Piel, C., and Alexandre, A.: ^{17}O-excess and d-excess of atmospheric water vapor measured by cavity ring-down spectrometry: Evidence of a matrix effect and implication for the calibration procedure, Rapid Commun. Mass Spectrom., 36, e9227, https://doi.org/10.1002/rcm.9227, 2022.

Wang, P., Yamanaka, T., Li, X. Y., Wu, X., Chen, B., Liu, Y., Wei, Z., and Ma, W.: A multiple time scale modeling investigation of leaf water isotope enrichment in a temperate grassland ecosystem, Ecol. Res., 33, 901–915, https://doi.org/10.1007/s11284-018-1591-3, 2018.

820 Wen, X. F., Zhang, S. C., Sun, X., Yu, G., and Lee, X.: Water vapor and precipitation isotope ratios in Beijing, China, J. Geophys. Res. Atmos., 115, 1–10, https://doi.org/10.1029/2009JD012408, 2010.

Yakir, D., Berry, J. A., Giles, L., and Osmond, C. B.: Isotopic heterogeneity of water in transpiring leaves: identification of the component that controls the $\delta^{18}O$ of atmospheric O_2 and CO_2, Plant. Cell Environ., 17, 73–80, https://doi.org/10.1111/j.1365-3040.1994.tb00267.x, 1994.

825 Zech, M., Mayr, C., Tuthorn, M., Leiber-Sauheitl, K., and Glaser, B.: Oxygen isotope ratios ($^{18}O/^{16}O$) of hemicellulose-derived sugar biomarkers in plants, soils and sediments as paleoclimate proxy I: Insight from a climate chamber experiment, Geochim. Cosmochim. Acta, 126, 614–623, https://doi.org/10.1016/j.gca.2013.10.048, 2014.